AWARD NUMBER: W81XWH-13-1-0009

TITLE: Defining Tumor Cell and Immune Cell Behavior in Vivo during Pulmonary Metastasis of Breast Cancer

PRINCIPAL INVESTIGATOR: Dr. Mark Headley

CONTRACTING ORGANIZATION: UNIVERSITY OF CALIFORNIA, SAN FRANCISCO
SAN FRANCISCO, CA 94103-4249

REPORT DATE: September 2015

TYPE OF REPORT: Annual

PREPARED FOR: U.S. Army Medical Research and Materiel Command
Fort Detrick, Maryland 21702-5012

REPORT DOCUMENTATION PAGE

Form Approved
OMB No. 0704-0188

1. REPORT DATE	2. REPORT TYPE	3. DATES COVERED
September 2015	Annual	1 Sep 2014 - 31 Aug 2015

4. TITLE AND SUBTITLE

Defining Tumor Cell and Immune Cell Behavior in Vivo during Pulmonary Metastasis of Breast Cancer

5a. CONTRACT NUMBER

5b. GRANT NUMBER
W81XWH-13-1-0009

5c. PROGRAM ELEMENT NUMBER

6. AUTHOR(S)

Mark Headley

E-Mail: mark.headley@ucsf.edu

5d. PROJECT NUMBER

5e. TASK NUMBER

5f. WORK UNIT NUMBER

7. PERFORMING ORGANIZATION NAME(S) AND ADDRESS(ES)

UNIVERSITY OF CALIFORNIA, SAN FRANCISCO 1855 FOLSOM ST STE 425 SAN FRANCISCO CA

8. PERFORMING ORGANIZATION REPORT NUMBER

9. SPONSORING / MONITORING AGENCY NAME(S) AND ADDRESS(ES)

U.S. Army Medical Research and Materiel Command
Fort Detrick, Maryland 21702-5012

10. SPONSOR/MONITOR'S ACRONYM(S)

11. SPONSOR/MONITOR'S REPORT NUMBER(S)

12. DISTRIBUTION / AVAILABILITY STATEMENT

Approved for Public Release; Distribution Unlimited

13. SUPPLEMENTARY NOTES

14. ABSTRACT

Metastasis is mediated by a complex set of factors, few of which are well understood. While a number of studies over the past several decades have linked function of the immune response to various outcomes in pulmonary metastasis it is currently poorly understood as to how immune cells engage with tumor cells to modulate metastatic success. Over the past two years we have defined a novel network using intravital lung imaging and flow cytometry by which early pioneer tumor cells release large numbers of tumor microparticles (cytoplasm containing blebs) into the lung circulation. We have found these microparticles are rapidly cleared from the lung by local immune cells. The outcome of this is loading of discrete immune populations such as Dendritic Cells with tumor antigen. These cells (dendritic cells specifically) subsequently act restrict successful metastasis.

15. SUBJECT TERMS

Lung Metastasis, Intravital Imaging, Tumor Immunology, Tumor Microparticles

16. SECURITY CLASSIFICATION OF:			17. LIMITATION OF ABSTRACT	18. NUMBER OF PAGES	19a. NAME OF RESPONSIBLE PERSON
a. REPORT	b. ABSTRACT	c. THIS PAGE			USAMRMC
Unclassified	Unclassified	Unclassified	Unclassified	34	19b. TELEPHONE NUMBER *(include area code)*

Standard Form 298 (Rev. 8-98)
Prescribed by ANSI Std. Z39.18

Table of Contents

Page

1) INTRODUCTION: Metastasis is mediated by a complex set of factors, few of which are well understood. While a number of studies over the past several decades have linked function of the immune response to various outcomes in pulmonary metastasis it is currently poorly understood as to how immune cells engage with tumor cells to modulate metastatic success. In this study we have sought to apply a novel method of microscopy to image lungs in live mice. This has allowed us for the first time to visualize the arrival of metastatic cells in the lung. Using this method we are currently evaluating the behaviors of Tumor cells themselves as well as the immune cells that interact with them in order to better understand the factors that dictate metastatic fitness in the lung.

2) KEYWORDS: *Metastasis, Intravital Imaging, Lung, Breast Cancer,*

3) ACCOMPLISHMENTS:

What were the major goals of the project?

Major Goals for Year 2:

1) Defining the Timeline of Cancer Cell Fate during pulmonary metastasis.

a) Characterization of Tumor Cell Behavior During Pulmonary Seeding via 2-photon microscopy

b) Characterization of Tumor and Immune Cell Interaction in Metastasis.

c) Definition of a timeline of tumor cell fate during lung metastasis.

2) Determine Requirement for VEGF Signaling During Pulmonary Metastasis

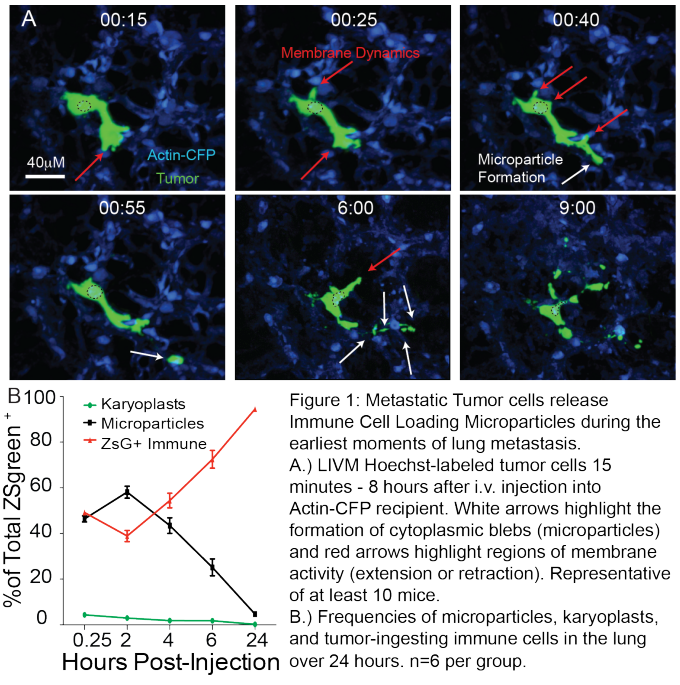

Figure 1: Metastatic Tumor cells release Immune Cell Loading Microparticles during the earliest moments of lung metastasis. A.) LIVM Hoechst-labeled tumor cells 15 minutes - 8 hours after i.v. injection into Actin-CFP recipient. White arrows highlight the formation of cytoplasmic blebs (microparticles) and red arrows highlight regions of membrane activity (extension or retraction). Representative of at least 10 mice. B.) Frequencies of microparticles, karyoplasts, and tumor-ingesting immune cells in the lung over 24 hours. n=6 per group.

What was accomplished under these goals?

Review of Year One Progress:

During Year One we significantly progressed our goals of applying live intravital imaging of the lung (LIVM) to the earliest moments of pulmonary metastasis and made our first forays into exploring how immune cells interact with

prospective metastatic cells during the earliest moments of metastasis. Key findings from this first year were that almost immediately upon entry into the lung metastatic tumor cells begin to shed large cytoplasmic blebs, which we have termed microparticles/cytoplasts and the parent tumor cells Karyoplasts (based on definitions of similar extracellular blebs in the literature.) **Figure 1A** shows examples images from one such imaging session where over the course of 8 hours you can readily see the tumor cell explore its local environment and shed microparticles. For the purposes of these imaging experiments we have utilized expression of a highly stable Fluorescent Protein(FP), ZsGreen, to label and allow visualization of the metastatic tumor cells. Importantly, use of this FP has an added benefit that if phagocytic immune cells encounter and ingest fragments of the tumor cell (such as these microparticles) the immune cell will retain that fluorescent signal enabling us to track cells that have encountered the tumor cell in this fashion. Quantification of these microparticles in combination with immune cells displaying the presence of the Zsgreen FP revealed a striking reciprocity between the appearance of these tumor-ingesting immune cells and the decline of the numbers of these microparticles within lung (Figure 1B.) At the culmination of the first year and leading into year two, our studies were focused on defining the nature of the immune cells which ingest these tumor microparticles and elucidating what possible function this interaction might have in the metastatic process.

Year 2 Progress:

1) <u>Defining the timeline of cancer cell fate during pulmonary metastasis</u>.

a. **Characterization of Tumor Cell Behavior** The bulk of our characterization of tumor cell behavior occurred during Year One and was previously described in the Year One Progress Report. However we did note several additional features during this subsequent year. After identification of the process of tumor microparticle formation and release by metastatic cells we became curious about the nature of these microparticles themselves. Importantly, their release is not dependent on apoptotic death of the tumor cell as inhibition of Caspases (blocking apoptotic death) does not impair microparticle generation and release (Figure 2A.) Also of note, the microparticles are significantly enriched for mitochondria (Figure 2B) suggesting they may in fact be metabolically active, though this remains to be determined

conclusively. However, in keeping with this, through intravital imaging of these microparticles following release from the tumor cells, we found that they retain the ability to migrate along the

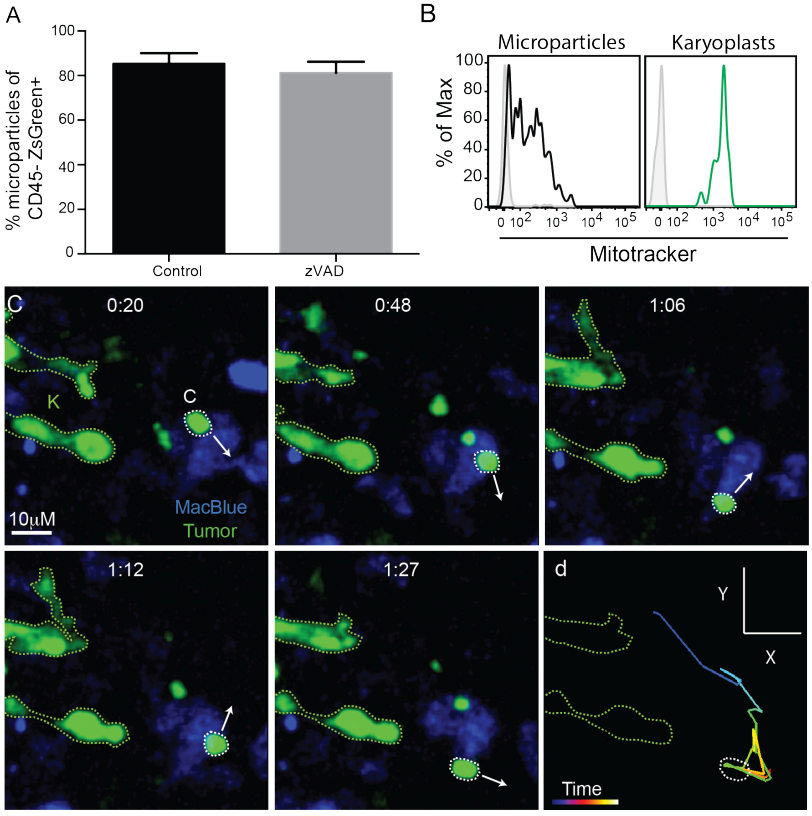

Figure 2: Tumor Microparticles are produced from viable tumor cells and retain autonomous migratory function.
A)Flow cytometric quantification of tumor microparticles in vivo from lung digests of mice treated with 10 μg ZVAD i.v at the time of injection with 2.5e5 ZsGreen+ Tumor cells. n=4 per group. no significant difference detected between groups by unpaired t test.
B)Mitotracker staining of Tumor Microparticles and Karyoplasts
C) Image series for tumor microparticle migrating autonomously through the lung microvasculature of a MacBlue host. Arrows represent the direction of the trajectory of the microparticlez at indicated timepoint. These data are representative of imaging collected from at least 12 mice.
D) Representative tracking of the microparticle in C.

vascular endothelium independent of the parental tumor cell from which they are released (Figure 2C).

b. Characterization of Tumor and Immune Cell Interaction in Metastasis.

The vast majority of our focus over the past year has been placed on exploring the nature of tumor and immune cell interaction during the earliest moments of metastasis as well as trying to elucidate what impact this has on metastatic success. In Year One we defined an interesting new phenomenon whereby immune cells putatively encountered Tumor-derived microparticles in the earliest moments of

metastasis and at least in some cases ingested those particles. Experimentally, this enabled us to trace immune cells that had ingested these particles based on the presence of the tumor expressed FP (ZsGreen) in these immune cells. We have termed these cells Tumor-Ingesting Immune Cells (TIICs). Over the past year we have better defined the identity of which immune cells make up the TIIC population and moreover now have some initial clues as to what effect ingestion has on these immune cells and metastatic success.

We first sought to determine whether tumor-microparticles in fact make up the tumor-derived entity ingested by the TIICs. In data previously shown in the Year One Progress report we had determined that the vast majority of TIICs display the surface marker CD11b (Figure 3A, as assessed by flow cytometry.) Expression of this marker strongly correlates with cells of the Myeloid lineage so we focused our studies on this portion of the immune population. We next returned to our LIVM method in order to directly image the moment of ingestion of tumor-microparticles by myeloid cells in the lung. We made use of the fluorescent reporter strain, MacBlue, which utilizes a Cyan Fluorescent Protein (CFP) driven by the monocyte and macrophage specific promoter *cfms* to specifically label these myeloid cells. We imaged these mice in combination with ZsGreen-expressing tumor cells between 2 and 6 hours after injection. As we hypothesized we found clear evidence that microparticles are targeted for ingestion by

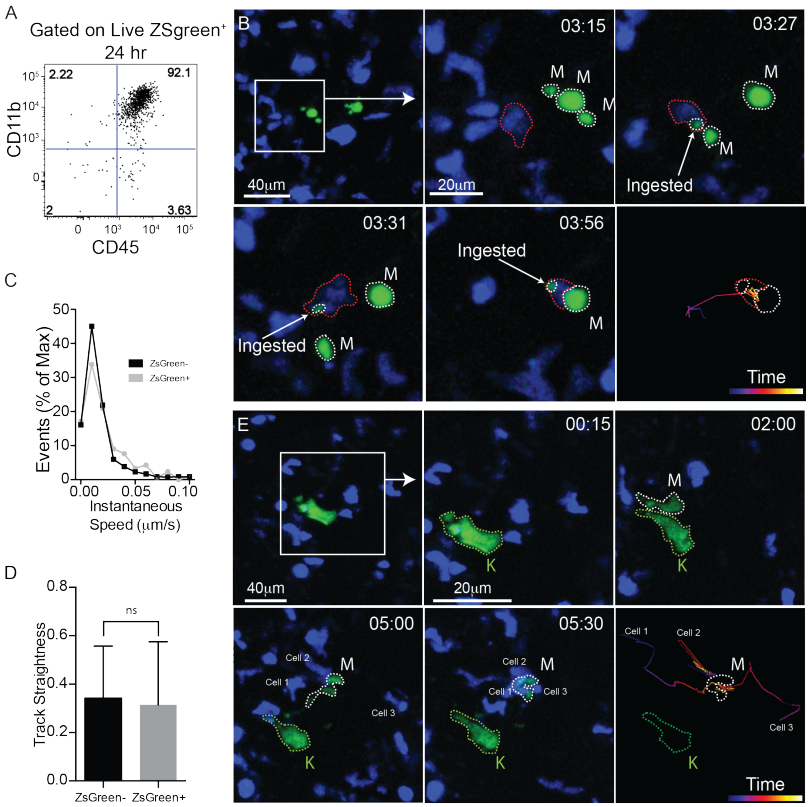

Figure 3: Encounter and Uptake of Tumor-Derived Microparticles by Lung Myeloid Cells
A.) Flow cytometry of CD11b+CD45+ cells in total Live ZsGreen+ population 24 hours post-injection.
B.) LIVM of microparticle phagocytosis by a CFP+ myeloid cell. Microparticles are outlined in white, and Microparticle ingesting cell in red. Final panel shows tracking data the ingesting cell. Representative of 5 mice.
C) Speed of microparticle-ingesting and non-ingesting cells. Data from 75 non-ingesting and 10 ingesting from 4 mice.
D.) Track straightness of Microparticle-ingesting and non-ingesting cells. Data from 75 non-ingesting and 10 ingesting from 4 mice.
E.) LIVM of CFP+ cell targeting microparticle. Karyoplasts are outlined in green and Microparticles are outlined in white. Tracked cells are labeled with Cell 1,2, or 3 in for comparison with tracks presented in final panel. Representative of 5 mice.

lung myeloid cells. Figure 3B shows a set of timelapse images from a movie of one microparticle from a grouping of three in the lung being targeted and ingested by a CFP+ myeloid cell. We next asked whether TIICs display unique behavioral properties as compared to those cells that haven't ingested tumor microparticles. As shown in Figure 3C and Figure 3D we find no evidence for differences in behavior, at least at the timepoints we are currently examining, either by instantaneous speed measurements (Figure 3C) nor straightness of track (Figure 3D.) The imaging in 3B initiated at a point where these three microparticles had already been produced, we were interested in observing the process in its entirety from production by the tumor cell to targeting by myeloids. Figure 3E shows an example of just such an event where the metastatic cell (in green) produces a very large microparticle over the course of several hours, following release of the microparticle, several CFP+ myeloid cells clearly target and "attack" this particle leaving the metastatic cell itself untouched. While this isn't a universal phenotype (we do see CFP+ cells in interaction with Karyoplasts as well) it is a very interesting idea that microparticles may in some cases serve as decoy's to distract the lung immune cells from the viable parental tumor cells, an idea we are interesting in testing more conclusively in the future.

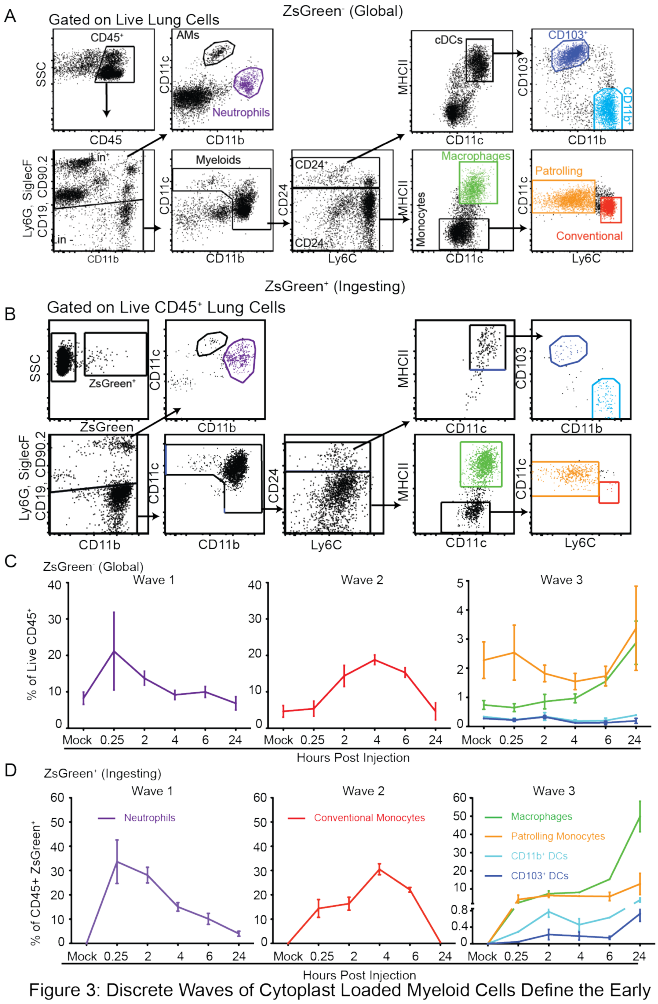

Figure 3: Discrete Waves of Cytoplast Loaded Myeloid Cells Define the Early Metastatic Niche
A.) Flow Cytometric Gating strategy for total lung myeloid populations.
B.) Flow Cytometric Gating strategy for tumor ingesting myeloids
C.) Frequency of myeloid cell in total lung cells over 24 hours following i.v. injection with B16ZsGreen. n=6
D.) Frequency of tumor-ingesting myeloid cells in the lung over 24 hours following i.v. injection with B16ZsGreen. n=6

The studies presented in Figure 3 support that microparticles serve as a platform for tumor loading of lung immune cells and may act to communicate specific information to those cells. We next asked exactly which immune cells encounter and ingest these microparticles over the first 24 hours within the lung. Using multi-parameter flow

cytometry we were able to define the majority of the myeloid cells of the lung. These populations include Alveolar Macrophages, Neutrophils, Conventional (Ly6c+) monocytes, Patrolling Monocytes, non-alveolar macrophages, CD103+ conventional Dendritic Cells, and CD11b+ conventional Dendritic Cells (Figure 4A). Importantly, through the use of ZsGreen positivity as a tracer for cells that have ingested microparticles we can use this same gating strategy (Figure 4B) to separately define changes in frequency in global (non-ingesting) immune cells versus ingesting immune cells over time. These data are shown in Figures 4C (Global) and 4D (Ingesting) over the first 24 hours. What was immediately striking to us, and novel to the field, was that the arrival and departure of the immune cells occurs in distinct waves. Initially both in Global and Ingesting populations there is a large influx of Neutrophils within 15 minutes of injection followed subsequently by a large increase in conventional monocytes between 2 and 4 hours. By 24 hours both of these waves have receded and the majority of cells retained within the ingesting pool are Macrophages (which prior literature would suggest differentiate from this initial wave of Monocytes[1,2], and our data support this.) Importantly, we additionally identify 3 other populations that make up this late wave none of which have previously been recognized as cells of interest in pulmonary metastasis. Patrolling monocytes are the most frequent secondary to Macrophages and a similar global enrichment can be observed. Interestingly, two populations of conventional dendritic cells (cDC, CD103+ and CD11b+) are enriched in this third wave of ingesting cells and there is no sign of enrichment in the global analysis (Figure 4C and 4D). This suggested to us that these cDC likely represent lung resident DC populations, in contrast to any of the other populations which are known to be recruited to the lung in response to injury of various sorts. To test this directly we utilized a method of intravascular labeling whereby anti-CD45 antibody is injected into the bloodstream just prior to euthanization and resection of lungs for FACs analysis (Figure 5A and [3]). Using this method, we found that all populations initially start out within the intravascular compartment of the lung (again indicative of recruited

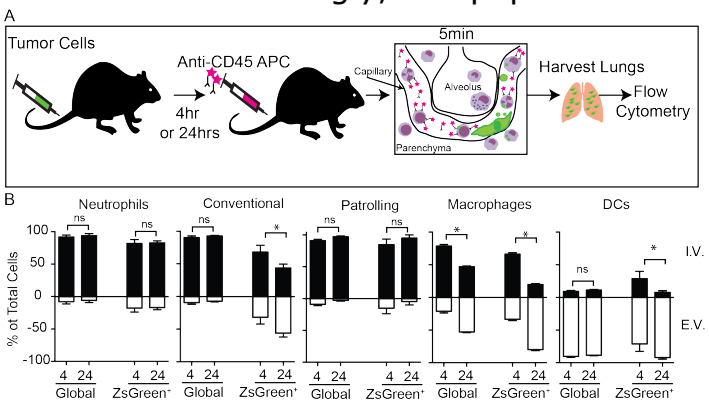

Figure 5: Vascular Localization of Tumor Ingesting Myeloid Cells
A.) Schema detailing method for discrimination of intravascular versus extravascular localization of lung myeloid populations
B.) Frequency of intravascular versus extravascular myeloid populations at 4 or 24 hours following i.v. injection of ZsGreen+ Tumor cells. n=6 per group. * is p< 0.05 using a Two-Way ANOVA with multiple comparison between row and column means.

circulating cells) with the exception of the two cDC populations which are extravascular throughout (Figure 5B, confirming their status as lung resident cells, at least during the timeframe of this metastatic event.)

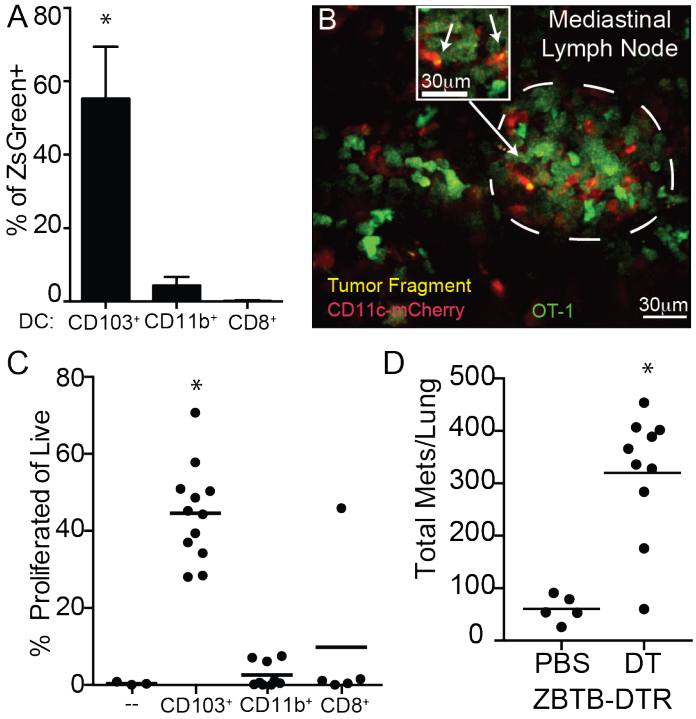

Figure 6 cDC restrict pulmonary metastasis
A.) Frequency of CD8+, CD11b+, and CD103+ DC in total ZsGreen+ cells in the mLN 72 hours post-injection. n=6 * is p< 0.05 using a One-Way ANOVA with Bonferroni Post-Test.
B.) Representative image of ZsGreen+CD11c-Cherry+ APC interacting with GFP-labeled OT-I T cells in a mLN 72 hours post-injection with ZSgreen+OVA+ Tumor cells. Inset highlights two ZsGreen-bearing CD11c+ cells in close interaction with OT1 T cells. n=3 mice.
C.) % proliferation of OVA-specific T cells cultured for 72 hours with indicated myeloid cells sorted from lung drain LN of mice 72 hours following injection of OVA-expressing tumor cells. n=6-12 per group from 2 experiments. * indicates p<0.05 from one way ANOVA with Bon Ferroni Post-Test.
D) Total # of lung metastases in PBS or DT treated Zbtb46-DTR bone marrow chimeras 2 weeks post-injection with Tumor Cells. n=5 for PBS and 10 for DT groups respectively. * p < 0.05 by unpaired t test.

Our finding that a previously unrecognized population of lung resident dendritic cells could be seen to interact with tumor and/or tumor-derived microparticles during these earliest moments of metastasis spurred our interest in investigating the function of these cells. CD103+ and CD11b+ DC are known to migrate out of the lung into the lung draining lymphnode in response to injury and infection as such we sought to determine if this is also the case during pulmonary metastasis. Indeed, flow cytometric analysis 72 hours after tumor cell injection revealed that a significant population of ZsGreen+ CD103+ DCs were present in of mediastinal (lung draining) LN (Figure 6A). Live imaging of LN at this timeframe in combination with antigen-specific CD8+ T cells revealed ZsGreen+ DC in close interaction with these T cells (Figure 6B). Further, *ex vivo* CD103+ DC were capable of robustly stimulating antigen-specific CD8+ T cells to proliferate while other LN myeloid cells failed

to do so (Figure 6C). Lastly and most importantly, we turned to a system that would allow us to specifically deplete cDC in order to interrogate directly the effect these cells have on pulmonary metastasis. We utilized a mouse strain whereby the cDC specific promoter *zbtb46* drives expression of the diphtheria toxin receptor (ZBTB46-DTR). Upon injection of diphtheria toxin (DT), cDC are systemically depleted within 24hours and lasting until ~72 hours[4]. Using this model system we depleted DC, 1 day prior to intravascular injection of Tumor cells. We quantified metastatic burden in lungs 2 weeks later comparing DC-replete and DC-depleted hosts. Strikingly, in the absence of conventional DC, metastatic burden was increased ~6-fold indicating that the interaction between this population and the tumor during these earliest hours of metastasis acts to restrict the successful implantation and growth of the metastatic cells (Figure 6D).

Taken as a whole in the past two years we have developed a novel approach to intravital lung imaging and applied this to visualize the arrival and behavior of metastatic cells in the lung for the first time. Using this methodology we have identified a generalized phenomena whereby metastatic cells release large numbers of microparticles into the lung circulation. These microparticles are encountered and ingested by local and recruited immune cells. At least one population of these immune cells, the cDC, utilizes the information contained in these blebs as antigen to mount an anti-tumor immune response and restrict the success of the burgeoning metastasis. We have submitted and recently gain acceptance of a manuscript at the journal Nature detailing these findings (more details on this provided in the appropriate section below.)

b. Definition of a timeline of tumor cell fate during lung metastasis.

In the data described above we have made great headway in defining a timeline of breast cancer metastasis. We now know the patterning of tumor cell entry into the lung, and how this is characterized both by release of microparticles and associated size reduction of the tumor cells. Further, these tumor cells undergo significant reduction in activity as they survive for longer durations in the lung becoming sessile. We also have defined a discrete wavelike network of immune cells that encounter and interact with the tumor cells both directly and through ingestion of tumor-derived microparticles. It remains to be determined how these events play out during spontaneous metastasis though we know from our studies that the lungs of mice bearing primary tumors do in fact bear microparticles and moreover tumor-loaded immune cells of similar identity to that seen in the more facile

IV injection model used for these studies. Future studies will help to bridge this gap.

2) Determine Requirement for VEGF Signaling During Pulmonary Metastasis

As stated above the bulk of this year was spent elaborating upon our findings with respect to the immune interaction with incoming metastatic cells. We submitted an initial version of a manuscript detailing these findings in March of 2015. Following receipt of reviews our attention was placed on responding to reviewer requests which took ~ 6 months of focused work. The manuscript was granted acceptance for publication at Nature in late December 2015. Due to this increased focus on this first manuscript our attention to the second major goal for this year was delayed.

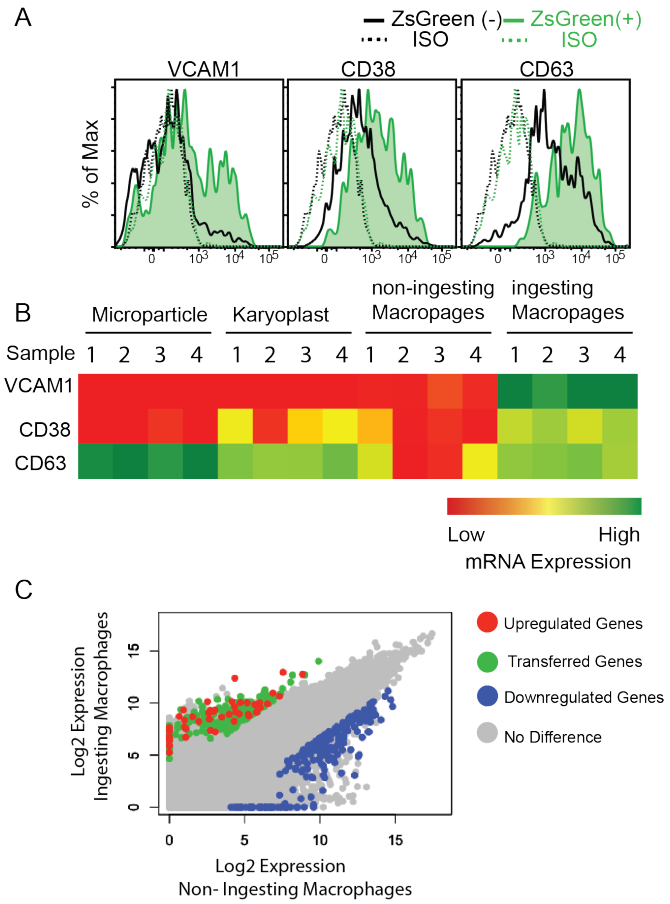

Figure 7: Characterization of gene expression changes in Macrophages that have ingested tumor microparticles.
A) Flow cytometric staining of ZsGreen+ and ZsGreen- Macrophages at 24hrs post-tumor injection. n=4.
B) Heatmaps for mRNA read-count taken from RNAseq of Tumor microparticles and Karyoplasts (2 hours post-injection into mouse) and non-ingesting and tumor-ingesting macrophages (24 hours post-injection). Data shown is for 4 samples per group with expression coded as a gradient from low (red) to mid(yellow) to high (green).
C) Comparison plot of gene expression between Ingesting and non-ingesting macrophages by RNAseq. Genes of intereste are colorcoded as either upregulated (Red), downregulated (Blue), putatively transferred from tumor cell to macrophage (Green), or no difference (grey).

However, the key element of this goal was less about specific interrogation of the role of the VEGF pathway in metastasis (though that is where our interest lay at the time of writing.) Moreso it was an Aim targeted at exploring how distinct molecular pathways may impact the process of metastasis and how this might be leveraged for better therapy (and explored through intravital imaging.) With this in mind we have actually made significant progress to this end though pursuit of this will require a request for change in the upcoming years goals and will be submitted soon after this progress report.
I would like to share some

of this data now. Largely this new potential direction comes from two sets of experiments. Firstly, in our efforts to characterize unique features of the tumor ingesting macrophages that we have defined above we undertook a broad flow cytometric staining panel to look at how surface markers are changed in this population compared to macrophages that have not ingested. Through this analysis we identified CD38, CD63 and VCAM as markers specifically upregulated on the tumor ingesting macrophages (Figure 7A). Additionally, we have performed RNAseq analysis comparing expression patterns of genes in tumor Karyoplasts, tumor Microparticles, non-ingesting macrophages, and tumor-ingesting macrophages. Through this analysis we made several key discoveries that form a centerpiece for what we would like to do moving forward. First off, examination of the three markers shown in Figure 7A revealed that while VCAM appears to be truly upregulated within the Macrophage population (Figure 7B). CD38 and CD63 both are highly expressed in the tumor populations themselves (Figure 7B). This is suggestive of the mRNA for these genes actually being transferred from the tumor cells to the macrophages and transcribed from there. We would like to address whether this is conclusively occurring in future studies. In addition to this we have generated a sizable panel of other genes of interest either upregulated within the Ingesting compartment , down-regulated, or possibly transferred from tumor to macrophage (Figure 7C). We are very interested in evaluating function of a subset these genes and are currently evaluating which genes are of greatest interest and likelihood for impact on metastatic fitness.

What opportunities for training and professional development has the project provided?

a) Local seminars, Lab Meetings, and Journal Clubs

- In keeping with our original training plan listed under the accepted Statement of Work I have attended regular seminar series and journal clubs held department wide here at UCSF. Additionally, I have presented findings from this project at several Krummel Lab-specific Lab meetings and attended Joint Lab Meetings held in combination with Dr. Zena Werb's group here at UCSF, Dr. Mark Looney's group, and a new joint lab meeting held between Dr. Charlie Kim's Group, Dr. Qizhi Tangs Group, and our own – I have presented at each of these joint lab meetings.
- Additionally, in the past year I have presented at a UCSF-wide Post-doctoral Seminar Series and as of May of this year have taken over as head organizer of this series. This requires networking with my post-doctoral peers as well as faculty at

UCSF in order to schedule speakers and coordinate the monthly seminar series itself.

- I also presented for the entirety of the UCSF and UC Berkeley Immunology community at the Annual InterDepartmental Immunology Retreat. The talk was titled "Visualization of Immediate Immune Responses To Pioneer Metastatic Cells In The Lung"

b) Meetings and Presentations

- February 2015 – I was invited to give a talk at the Photonics West Conference titled "Probing *in vivo* Dynamics In The Early Metastatic Niche In the Lung". The emphasis of this talk being, our lung intravital imaging methodology and its application to the study of metastasis.

- March 2015- During this second year of the project I attended the Keystone Meeting on Macrophages and Dendritic Cells Reunited. This meeting was chosen both due to a strong emphasis on these myeloid populations in Cancer within the presenters at the meeting. But also as my own project become more focused on these very same populations it was an excellent opportunity to meet leaders in these fields. I presented a poster at this meeting.

- September 2015 – I was an invited speaker at the World Molecular Imaging Congress in the Educational Session on Cancer Immunology. I gave a talk entitled " Harnessing Intravital Microscopy To Understand The Real-Time Dynamics of Immune Cells in The Tumor Microenvironment."

c) Teaching, Mentoring, and Management Skill Building

- During this time I served as a session lead for the UCSF Medical School Article Discussion Group. This involved leading a group of second year medical students in analyzing and discussing papers of interest to Cancer Immunotherapy.

- Additionally during this past year I mentored a technician within our group who has assisted on this project. The bulk of her training occurred in year one but during this time greater emphasis was placed on moving her towards independence as a researcher. She has now left our lab to begin Medical School here at UCSF.

- I additionally mentored a Rotation student within our lab on a project not directly related to what was described in the report but focused on interrogating the function of the cytokine IL-33 in pulmonary metastasis.

- Lastly, I participated in the UCSF Scientific Leadership and Management Course and 2 day workshop designed to build Managerial skills and tools.

5) How were the results disseminated to communities of interest?

Results from these projects were disseminated to broader communities at the Keystone Conference on Macrophages and Dendritic Cells, The Photonics West Conference, and The World Molecular Imaging Conference.
Additionally, associated with the acceptance and publication of our paper in March of 2016 the UCSF PR department released a press release/article to a variety of news organizations, this was also posted on the UCSF Facebook page and UCSF Website and will be followed soon by a short annotated movie describing the work posted to these same sites.

6) What do you plan to do during the next reporting period to accomplish the goals?

Over the past two years we have largely addressed the major goals for our analysis of how the immune system and metastatic cells interact during the earliest phases of metastasis. We have seen this work through to a publication in Nature.

Our focus on this publication (in combination with an initial delay in Year One as we refined our imaging platform) has somewhat delayed our foray into molecular features of this process. However through the studies we have undertaken we have gained a great deal of new insight into which molecular pathways are of interest to explore as described above and in Figure 7. In the coming and final year we would like to pursue function of a subset of the genes we have found to be altered in tumor-ingesting macrophages. This would represent a goal change for Year 3 from what was originally proposed in our Statement of Work and we will be writing for formal permission to

make this adjustment.

Year 3 also marks the timeframe for an additional set of goals to define how the adaptive immune response functions in metastasis. We have tools in place and to begin these studies now and will be pursuing them alongside our modified plans for addressing molecular pathways in metastasis.

7) IMPACT:

a) What was the impact on the development of the principal discipline(s) of the project?

As part of these studies we have been able to directly observe, for the first time, the arrival of a metastatic tumor cell into the lung. Through this initial observation we have identified a new pathway by which tumor cells shed excess cytoplasm in the lung vasculature (through production of tumor microparticles.) By tracing the fate of these particles we have identified that Lung cDC represent a population of resident cells actively opposing metastatic success. This has the potential for great impact on the field of pulmonary metastasis as this population has not previously been shown to interact with burgeoning metastases and our finding indicates this may be a population of cells that can be leverage for therapy in the future.

b) What was the impact on other disciplines?

Nothing to report with respect to impact on other disciplines from this year of study. However, our continued refinement of intravital lung imaging methodology (as reported in Year One) continues to be an area of interest for laboratories studying various aspect of lung immunology and pathology and we have trained several additional groups in the use of this method over the past year.

c)What was the impact on technology transfer?

Nothing to Report.

d) What was the impact on society beyond science and technology?

Nothing to Report

8) CHANGES/PROBLEMS:

a) Changes in approach and reasons for change

Nothing to Report

b) Actual or anticipated problems or delays and actions or plans to resolve them

During the early portion of Year 2 (March) we submitted a manuscript on the described work to Nature and received favorable reviews. Addressing reviewer requests took approximately 6 months after which in December of 2015 the paper was accepted for publication and was published in Nature in March of 2016. Due to this process our studies focused predominantly on Major Goal One throughout the year as this was the focus of this publication. This has delayed work on Major Goal 2. We will be submitting a request for change regarding this specific goal as our work in Major Goal One has yielded significant progress in identifying additional molecular targets of interest as describe above.

c. Changes that had a significant impact on expenditures

Nothing to Report

e) Significant changes in use or care of human subjects, vertebrate animals, biohazards, and/or select agents

f) Significant changes in use or care of human subjects

Nothing to Report/Not Applicable

g) Significant changes in use or care of vertebrate animals.

Nothing to Report

h) Significant changes in use of biohazards and/or select agents

Nothing to Report

9) PRODUCTS:

a) *Publications, conference papers, and presentations*

i. ***Journal publications.***

One journal publication has resulted from these work.

Mark Headley, Adriaan Bins, Alyssa Nip, Edward Roberts, Mark R Looney, Audrey Gerard, Matthew Krummel; Visualization of immediate immune responses to pioneer metastatic cells in the lung.; Nature; 531:2016; 513-517; published; acknowledgment of federal support: YES

ii. ***Books or other non-periodical, one-time publications.*** Nothing to Report

iii. **Other publications, conference papers, and presentations.** Nothing to Report

b) *Website(s) or other Internet site(s)* Nothing to report

c) *Technologies or techniques*

Refined approach to Lung Intravital Microscopy (LIVM.) This approach was described in detail in the publication listed above. Additionally, we have already shared this revised method with several other researchers onsite at UCSF as well as external labs with whom we'd previously trained in the former lung imaging methodology. We will freely train and or share knowledge with other groups interested in this method.

d) *Inventions, patent applications, and/or licenses*

Nothing to Report

e) *Other Products*

Nothing to report

10) PARTICIPANTS & OTHER COLLABORATING ORGANIZATIONS

What individuals have worked on the project?

i. Name: Mark Headley – no change

ii. Name: Alyssa Nip – No Change

iii. Name: Adriaan Bins

Person Hour Worked 2 months

Contribution to Project: Assisted in Lung Intravital Imaging Method

Funding: NIH

iv. Name: Edward Roberts

Person Hour Worked: 1 Month

Contribution to Project: Generated Mouse Embryonic Fibroblast Cell lines

Funding: NIH

v. Name: Audrey Gerard

Person Hour Worked: 1 month

Contribution to Project: Participated in Lung LN Imaging

Funding: NIH

11) References

1 Qian, B. *et al.* A distinct macrophage population mediates metastatic breast cancer cell extravasation, establishment and growth. *PLoS One* **4**, e6562, doi:10.1371/journal.pone.0006562 (2009).

2 Qian, B. Z. *et al.* CCL2 recruits inflammatory monocytes to facilitate breast-tumour metastasis. *Nature* **475**, 222-225, doi:10.1038/nature10138 (2011).

3 Anderson, K. G. *et al.* Intravascular staining for discrimination of vascular and tissue leukocytes. *Nature protocols* **9**, 209-222, doi:10.1038/nprot.2014.005 (2014).

4 Meredith, M. M. *et al.* Expression of the zinc finger transcription factor zDC (Zbtb46, Btbd4) defines the classical dendritic cell lineage. *J Exp Med* **209**, 1153-1165, doi:10.1084/jem.20112675 (2012).

12) APPENDICES: Nature Journal Article attached

LETTER

doi:10.1038/nature16985

Visualization of immediate immune responses to pioneer metastatic cells in the lung

Mark B. Headley[1], Adriaan Bins[1,2], Alyssa Nip[1], Edward W. Roberts[1], Mark R. Looney[3], Audrey Gerard[1] & Matthew F. Krummel[1]

Lung metastasis is the lethal determinant in many cancers[1,2] and a number of lines of evidence point to monocytes and macrophages having key roles in its development[3–5]. Yet little is known about the immediate fate of incoming tumour cells as they colonize this tissue, and even less known about how they make first contact with the immune system. Primary tumours liberate circulating tumour cells (CTCs) into the blood and we have developed a stable intravital two-photon lung imaging model in mice[6] for direct observation of the arrival of CTCs and subsequent host interaction. Here we show dynamic generation of tumour microparticles in shear flow in the capillaries within minutes of CTC entry. Rather than dispersing under flow, many of these microparticles remain attached to the lung vasculature or independently migrate along the inner walls of vessels. Using fluorescent lineage reporters and flow cytometry, we observed 'waves' of distinct myeloid cell subsets that load differentially and sequentially with this CTC-derived material. Many of these tumour-ingesting myeloid cells collectively accumulated in the lung interstitium along with the successful metastatic cells and, as previously understood, promote the development of successful metastases from surviving tumour cells[3]. Although the numbers of these cells rise globally in the lung with metastatic exposure and ingesting myeloid cells undergo phenotypic changes associated with microparticle ingestion, a consistently sparse population of resident conventional dendritic cells, among the last cells to interact with CTCs, confer anti-metastatic protection. This work reveals that CTC fragmentation generates immune-interacting intermediates, and defines a competitive relationship between phagocyte populations for tumour loading during metastatic cell seeding.

Primary tumours induce distal accumulation of immune cells in the lung that promotes metastasis[4,5]. B16F10 subcutaneous tumours, expressing ZsGreen (hereafter referred to as B16ZsGreen), resulted in $CD45^+ZsGreen^+$ (immune) cells in the lung before the appearance of micrometastases (Fig. 1a, b). These cells contained vesicular $ZsGreen^+$ puncta, suggesting ingestion of tumour fragments (Fig. 1c). An experimental metastasis model, intravenous (i.v.) injection of B16ZsGreen cells, revealed similar loading of intracellular vesicles in $CD45^+$ cells over 24 h (Extended Data Fig. 1a–c). Notably, $CD45^+ZsGreen^+$ cells increased rapidly within 4 h after injection, and exceeded the initial frequency of the B16ZsGreen cells (Extended Data Fig. 1c), suggesting a cell-fragment origin of ingested tumour material. These $CD45^+ZsGreen^+$ cells again had puncta of ingested tumour material (Extended Data Fig. 1d).

Previous work has established roles for primary tumour-derived exosomes ($\leq$200 nm in diameter) in the lung pre-metastatic niche[7]. However, the size of inclusions within sorted $CD45^+ZsGreen^+$ cells (diameters often $\geq$1 μm (Fig. 1c and Extended Data Fig. 1d)) suggested that this might occur via a distinct mechanism. As CTCs are detectable in the blood of patients with metastatic disease[8], we sought to visualize their fate upon entering the lung vasculature. To image the arrival of injected B16ZsGreen metastatic cells in lung capillaries, we updated our published method for lung intravital microscopy (LIVM)[6] using a novel intercostal window (Extended Data Fig. 2a–e) allowing for stable imaging of $\leq$12 h (Extended Data Fig. 2f). Figure 1d and Supplementary Video 1 show that within seconds of arrival, the incoming CTCs became lodged in capillaries and began to shed microscale blebs (microparticles) into the vasculature.

Microparticle generation was observed repeatedly over at least 8 h after injection (Fig. 1e and Supplementary Video 2). These blebs had an average diameter of 5 μm, with a range of 0.5 to >25 μm (Fig. 1f), markedly larger than exosomes and larger than most previously reported microparticles[9]. Arrested B16ZsGreen cells were also observed to undergo membrane protrusion and retraction (Supplementary Video 2 and Extended Data Fig. 3a). Over time, surviving tumour cells decreased in size and the protrusive activity reduced (Extended Data Fig. 3a–c and Supplementary Video 3). In most instances of microparticle release, the nucleus of the parent cell maintained integrity and the blebs themselves retained the cytoplasmic fluorophore, consistent with non-apoptotic blebbing[10]. We also observed cells undergoing lysis (Supplementary Video 4), distinguished from apoptosis by a lack of blebbing and rapid loss of the cytoplasmic fluorophore. On the basis of these criteria, we adopted the terminology for parental nucleated cells as 'karyoplasts' and the blebs as 'cytoplasts'.

Previous lung explant and slice imaging studies did not reveal the generation of cytoplasts during metastasis[11,12]; we hypothesized that their formation was dependent on shear forces in intact lungs. We compared the behaviour of tumour cells in LIVM versus slice to test this[13]. In the non-shear system, the production of cytoplasts was approximately fourfold reduced (Fig. 1g). Further, cytoplast production was unaltered in the presence of the apoptosis inhibitor Z-VAD (Extended Data Fig. 4a, b). This demonstrates that cytoplast formation is driven by physical forces rather than a programmed cell death mechanism. In LIVM, many microparticles also exhibited autonomous motility, with spontaneous arrest and adherence on vascular walls (Supplementary Video 5) and migration against vascular flow (Extended Data Fig. 4c–e and Supplementary Video 6). The speed of these particles was around 10 μm min^{-1} in the absence of vascular flow, and an order of magnitude faster in LIVM (Fig. 1h).

Having observed the generation process *in vivo*, we developed a flow cytometric assay to study their formation and fate. Using Hoechst-staining to accurately differentiate karyoplasts from cytoplasts (confirmed by confocal imaging), we found that cytoplasts became the dominant tumour-cell-derived species within the lung within 15 min (Fig. 1i, j and Extended Data Fig. 3d). Cytoplasts contained mitochondria (Fig. 1k, l and Extended Data Fig. 3e), consistent with retention of metabolic potential and motility. The production of these particles was not unique to *in vitro* passaged B16F10 cells, as robust cytoplast generation was seen with B16ZsGreen cells

[1]Department of Pathology, University of California, San Francisco, 513 Parnassus Ave, HSW512, San Francisco, California 94143-0511, USA. [2]Department of Medical Oncology, Academic Medical Center Amsterdam, Meibergdreef, 91105AZ Amsterdam, The Netherlands. [3]Departments of Medicine and Laboratory Medicine, University of California, San Francisco, 513 Parnassus Avenue, HSW512, California 94143-0511, USA.

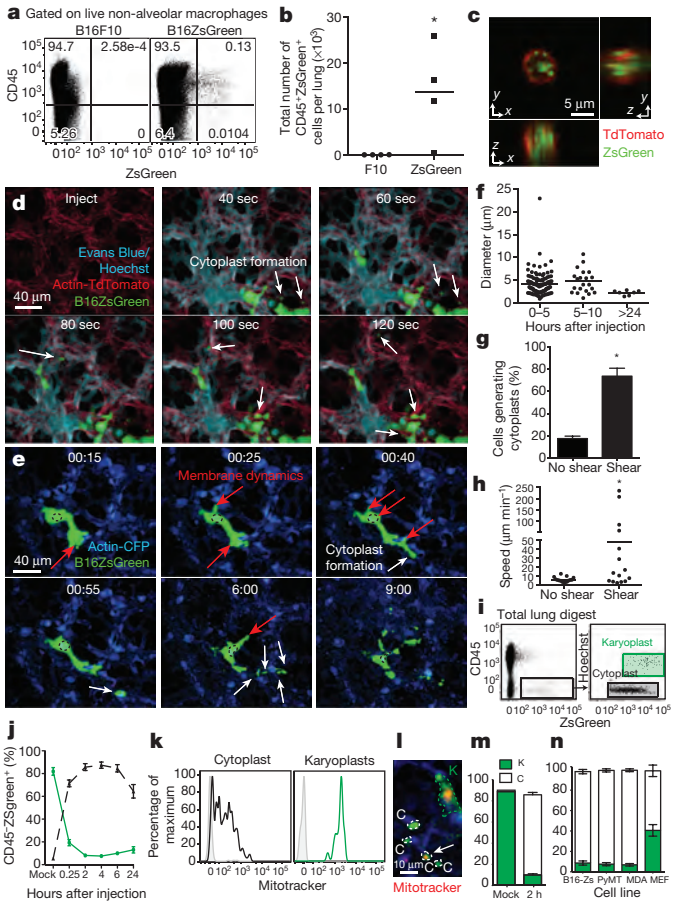

Figure 1 | Intravital imaging of the first hours of lung seeding by B16 melanoma. a, Representative plots of CD45$^+$ZSgreen$^+$ cells in lungs of mice bearing 2-week primary B16 melanoma tumours with or without ZsGreen expression. Alveolar macrophages were excluded, as auto-fluorescent signal interfered with ZsGreen discrimination. **b**, Absolute number of CD45$^+$ZsGreen$^+$ and CD45$^-$ZsGreen$^+$ cells in lungs from **a**. *$P = 0.0421$ by unpaired *t*-test. **c**, Confocal imaging of sorted CD45$^+$ZsGreen$^+$ cells from lungs of mTmG mouse (with ubiquitous expression of membrane-bound TdTomato) bearing tumours as per **a**. Red, TdTomato; green, ZsGreen. **d**, **e**, LIVM after i.v. injection of Hoechst-labelled B16ZsGreen cells into mTmG mice with Evan's Blue labelling vascular flow (see also Supplementary Video 1) (**d**). LIVM Hoechst-labelled B16ZsGreen cells from 15 min to 9 h after i.v. injection into actin–CFP recipient (see also Supplementary Video 2) (**e**). White arrows highlight the formation of cytoplasmic blebs (cytoplasts) and red arrows highlight regions of membrane activity (extension or retraction). Representative of at least 10 mice. **f**, Cytoplast diameter at 0–5 h, 5–10 h and >24 h after injection. **g**, Percent cytoplast producing B16ZsGreen cells from non-shear (slice imaging) or shear (LIVM) (15 cells per group from 3 mice; *$P = 0.002$ by unpaired *t*-test). **h**, Cytoplast speed in non-shear or shear conditions as **f** (15 cytoplasts per group in 3 mice; *$P = 0.036$, unpaired *t*-test). **i**, Gating strategy for karyoplast and cytoplast discrimination within lung single-cell suspension. **j**, *In vivo* mean cytoplast and karyoplast frequency in lung ($n = 6$ per group). **k**, Mitotracker staining of cytoplasts and karyoplasts. **l**, LIVM of mitotracker labelled B16ZsGreen cells. **m**, *In vivo* cytoplast frequency in lung 2 h after injection of primary-isolated B16ZsGreen cells or mock injected. Green, karyoplasts; white, cytoplasts. $n = 4$ per group. **n**, *In vivo* cytoplast frequency 2 h after injection of B16ZsGreen, murine breast tumour (PyMT-B), human breast tumour (MDA-MB-231), and non-transformed primary mouse embryonic fibroblasts ($n = 3$ per group from 2 experiments). Horizontal bars represent means, error bars are s.d.

isolated directly from primary subdermal tumours and re-injected i.v. (Fig. 1m), a mouse breast tumour line (PyMT-B), human MDA-MB231 breast tumour cells, and non-transformed mouse embryonic fibroblasts (Fig. 1n).

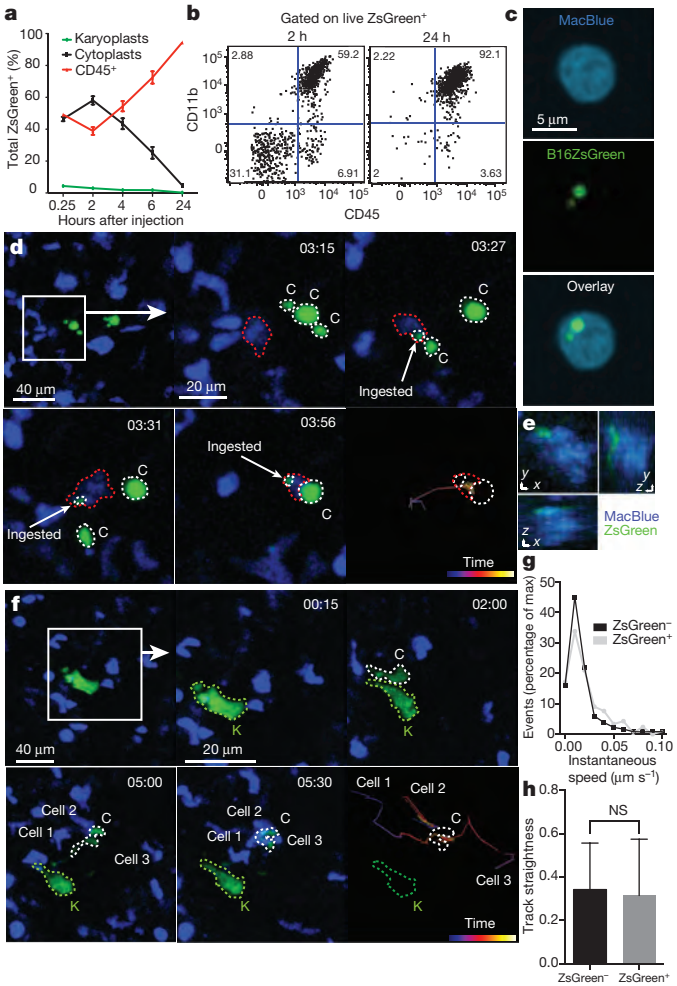

Figure 2 | Encounter and uptake of tumour-derived cytoplasts by lung myeloid cells. a, Frequencies of cytoplasts, karyoplasts, and CD45$^+$ZsGreen$^+$ cells in the lung over 24 h ($n = 6$ per group). **b**, Flow cytometry of CD11b$^+$CD45$^+$ cells in total ZsGreen$^+$ population 2 and 24 h after injection. **c**, Confocal imaging of CD45$^+$ZsGreen$^+$ cells from MacBlue mice 24 h after injection. **d**, LIVM of cytoplast phagocytosis by a CFP$^+$ myeloid cell (see also Supplementary Video 7). Green, karyoplasts; white, cytoplasts; red, cytoplast ingesting cell. Rightmost panel shows tracking data for a subset of cells. Representative of 5 mice. **e**, *xy*, *yz* and *xz* renders of CFP$^+$ myeloic cell from **d**. **f**, LIVM of CFP$^+$ cell targeting cytoplast (see also Supplementary Video 8). Colours and tracking as in **d**. Tracked cells labelled as cell 1, 2 or 3 in **f** for comparison with tracks. Representative of 5 mice. **g**, Speed of cytoplast-ingesting and non-ingesting cells. **h**, Track straightness of cytoplast-ingesting and non-ingesting cells. Data from 75 non-ingesting and 10 ingesting cells from 4 mice, error bars are s.d.

The number of cytoplasts peaked by 4 h, with few detectable by 24 h. Meanwhile, karyoplast number declined according to a one-phase exponential decay over the first day with a half-life ($t_{1/2}$) of 6.3 h (Fig. 2a). Comparison of the frequency of immune-associated ZsGreen$^+$ events with that of free cytoplasts and karyoplasts revealed a strong reciprocal relationship between the rise in ZsGreen$^+$ immune cells and loss of free cytoplasts (Fig. 2a). This suggested that cytoplasts represent the source of ingested tumour material in pre-metastatic lungs. Myeloid cells were implicated as the primary phagocytes on the basis of CD11b expression (Fig. 2b). Assessment of the myeloid lineage reporter MacBlue (eCFP (enhanced cyan fluorescent protein) expression driven by a modified *CFMS* promoter cassette, labelling monocytes and monocyte-derived cells, as well as a small portion of neutrophils)[14] further revealed CFP$^+$ZsGreen$^+$ cells containing ingested tumour fragments (≥1 μm diameter), consistent with cytoplast

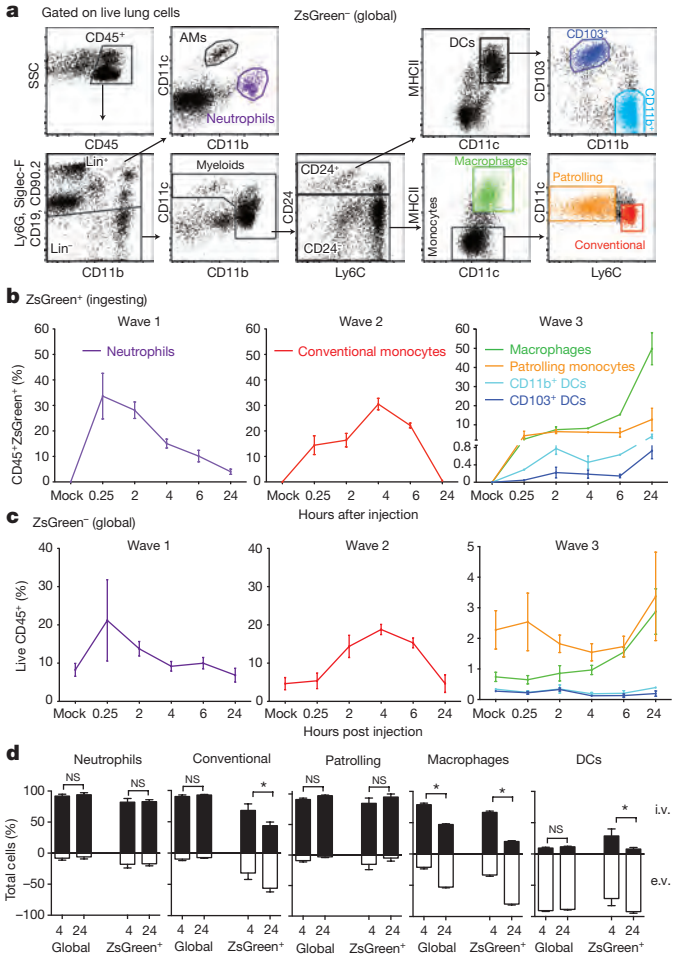

Figure 3 | Discrete waves of cytoplast loaded myeloid cells define the early metastatic niche. a, Gating strategy for total lung myeloid populations. **b**, Frequency of tumour-ingesting myeloid cells in the lung over 24 h following i.v. injection with B16ZsGreen ($n = 6$). **c**, Frequency of myeloid cells in total lung cells over 24 h following i.v. injection with B16ZsGreen ($n = 6$). **d**, Frequency of intravascular versus extravascular myeloid populations at 4 or 24 h following i.v. injection of B16ZsGreen cells ($n = 6$ per group; $^*P < 0.05$, two-way ANOVA with multiple comparison between row and column means). Error bars are s.d.

uptake (Fig. 2c). Importantly, using LIVM, we were able to observe CFP$^+$ cells directly ingesting cytoplasts (Fig. 2d, e and Supplementary Video 7). Additionally, we occasionally observed swarming by CFP$^+$ cells following release of a cytoplast from a parental karyoplast with these cells ignoring the neighbouring viable karyoplast (Fig. 2f and Supplementary Video 8). A bias of phagocytes towards cytoplasts was not universal and CFP$^+$ cells were also frequently found in direct interaction with karyoplasts (Supplementary Video 9), although in hundreds of hours of imaging, we never observed phagocytosis of an intact karyoplast. Evaluation of the behavioural characteristics of cytoplast-ingesting versus non-ingesting myeloid cells revealed no clear differences in either instantaneous speed nor path straightness, although the latter would be heavily dictated by the vasculature (Fig. 2g, h). Taken together, these data support the hypothesis that pioneer CTCs generate cytoplasts within the lung vasculature early on arrival in the lung, leading to loading of local phagocytes.

We next characterized the identity of the tumour-ingesting myeloid cells in the early metastatic niche using flow cytometry (Fig. 3a and Extended Data Fig. 5a). Our analysis included specific gating of alveolar macrophages (Siglec-F$^+$, CD11c$^+$, CD11b^{low}), neutrophils (Ly6G$^+$, Ly6C$^+$, CD11b$^+$), conventional monocytes (Ly6C$^+$, CD11b$^+$, MHCII$^{+/-}$, Ly6G$^-$, CD11c$^-$, CD24$^-$), patrolling monocytes (CD11b$^+$, CD11c^{mid}, Siglec-F$^-$, Ly6G$^-$, MHCII$^-$, CD24$^-$, Ly6C$^{low/-}$), non-alveolar macrophages (CD11b$^+$, CD11c$^+$, MHCII$^+$, CD24$^-$, Siglec-F$^-$, Ly6G$^-$) and two populations of lung-resident conventional dendritic cells (cDCs): CD103$^+$ and CD11b$^+$ (CD24$^+$, CD11c$^+$, MHCII^{hi}, Ly6C$^-$, CD103$^+$ or CD11b$^+$). Both monocyte populations expressed CD115, and macrophages, but not cDCs, expressed CD64 and F4/80, supporting the definitions of these populations (data not shown). Using this strategy, we examined lungs across a 24 h time course, gating on ZsGreen$^-$ (Fig. 3a) or ZsGreen$^+$ (Extended Data Fig. 5a) cells to understand the dynamics of total versus cytoplast-loaded myeloid populations. This revealed a progressive wavelike shift in the identity of myeloid cells that contained CTC-derived material (ZsGreen$^+$) (Fig. 3b, c). The first wave was dominated by neutrophil uptake, occurring within 15 min of injection, peaking around 30 min and returning to near-baseline by 24 h. Wave 2 was dominated by loading of conventional monocytes with a peak at 4 h followed by a return to baseline by 24 h. Finally, wave 3 established between 6 and 24 h comprised of non-alveolar macrophages, patrolling monocytes and DCs. Among those, non-alveolar macrophages were the most numerous, representing greater than 60% of total CD45$^+$ZsGreen$^+$ cells at 24 h, followed by patrolling monocytes and both CD103$^+$ DCs and CD11b$^+$ DCs at much lower frequencies (Fig. 3b). These waves were largely mirrored in global (ZsGreen$^-$) populations with the notable exception of the DC populations (Fig. 3c), consistent with uptake frequency being largely a function of cellular frequency.

We next sought to determine how cytoplast-ingesting cells behaved with respect to extravasation. We used i.v. injection of labelled anti-CD45 antibody[15] to localize ZsGreen$^+$ populations relative to the vasculature at 4 and 24 h after injection. Consistent with previous data[3], non-alveolar macrophages extravasated over this time period (Fig. 3d and Extended Data Fig. 5b–d). Interestingly, a portion of ZsGreen$^+$ conventional monocytes also extravasated, consistent with recent reports that this population can exit circulation without differentiation into macrophages[16]. In contrast, tumour-loaded patrolling monocytes and neutrophils remained intravascular throughout. The DC populations that gathered tumour material remained largely extravascular throughout, with the exception of a very small but consistent population of ZsGreen$^+$ DCs, at 4 h, that stained for i.v. CD45, which may reflect intravascular sampling by these DC populations (Fig. 3d).

It is likely that some elements of this wave structure are influenced by the bolus nature of the i.v. injection model in contrast to the more continual release of CTCs expected in spontaneous metastasis. Although it is currently difficult to catch cells arriving from a spontaneous tumour, we hypothesize that these waves would exist as a continuum; indeed, the cytoplast-containing cells in lungs of mice bearing primary tumours were dominated by monocytes and macrophages (Extended Data Fig. 5e). Nonetheless, these data suggest that a dichotomy exists in the behaviour of recruited versus lung-resident myeloid populations during metastasis.

Multicolour imaging at 24 h confirmed previous observations[4] that monocyte and monocyte-derived cells (CFP$^+$) and not DCs were dominant in a successful early metastasis (Fig. 4a). Using B16ZsGreen cells, our study extends those observations by showing that these cells contain ingested ZsGreen$^+$ tumour material. This suggests that some originated as cytoplast-ingesting cells (Fig. 4b). Live-imaging of these nascent metastases showed relatively stable and non-motile myeloid cells, although a few underwent directional migration towards micrometastases (Fig. 4c, d). Notably, ZsGreen$^+$ macrophages displayed unique upregulation of a variety of adhesion and chemotactic receptors, relative to ZsGreen$^-$ or steady-state macrophages (Fig. 4e). This provides evidence that tumour ingestion and interaction drives these cells down a distinct activation pathway.

The loaded DC wave at 24 h suggested the potential for an immune-stimulatory fate for some tumour-derived material. Flow-cytometric analysis of antigen-presenting cell (APC) populations

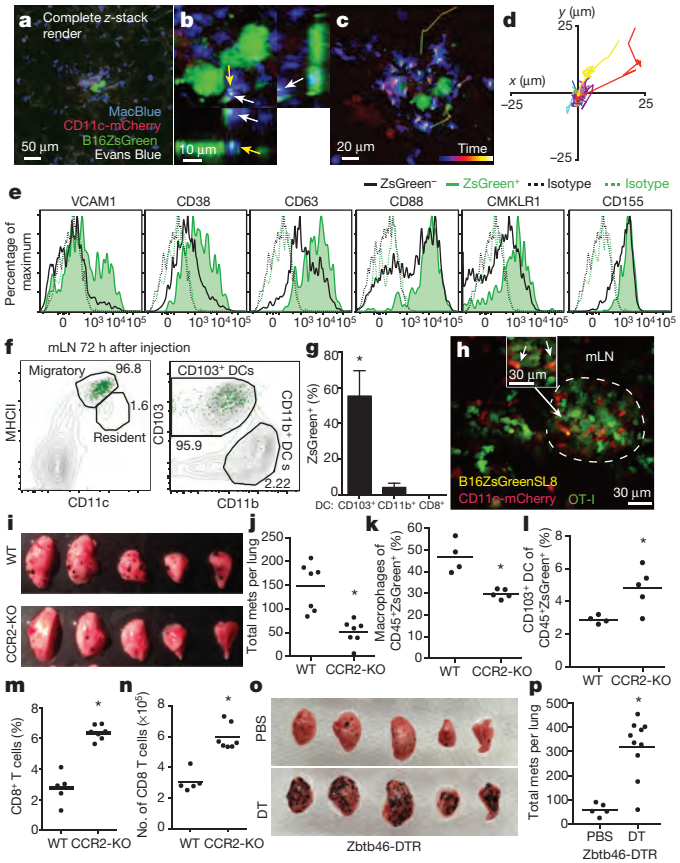

Figure 4 | Lung-resident dendritic cells inhibit metastasis of B16 melanoma. **a**, Maximum intensity projection of LIVM of B16ZsGreen tumour 24 h after injection into CD11c-mCherry MacBlue host (see also Supplementary Video 9). Representative of 5 mice. **b**, High magnification showing tumour-loaded MacBlue$^+$ cells in close interaction with B16ZsGreen cell at 24 h after injection. **c**, Representative image from time-lapse. Track overlays describe motion of tracked MacBlue$^+$ cells over a period of ~1 h. **d**, Overlay of 10 tracks of MacBlue$^+$ cells from **c**. **e**, Staining of ZsGreen$^+$ and ZsGreen$^-$ macrophages 24 h after tumour injection ($n = 4$). **f**, Gating of lung-draining mLN 72 h after injection. Contour lines, total LN; green dots, ZsGreen$^+$ cells. **g**, Frequency of CD8$^+$, CD11b$^+$ and CD103$^+$ DCs in total ZsGreen$^+$ cells in the mLN 72 h after injection. ($n = 6$; $^*P < 0.05$, one-way ANOVA with Bonferroni post-hoc test). **h**, Representative image of ZsGreen$^+$CD11c-mCherry$^+$ APCs interacting with GFP-labelled OT-I T cells in a mLN 72 h after injection with B16ZsGreenSL8 (see also Supplementary Video 10). Inset highlights two ZsGreen-bearing CD11c$^+$ cells in close interaction with OT-I T cells ($n = 3$ mice). **i**, Representative images of metastasis-bearing lungs from wild-type (WT) or CCR2-knockout (KO) mice 2 weeks after injection with B16ZsGreen. **j**, Total number of lung metastases (mets) in wild-type and CCR2-knockout mice 2 weeks after injection with B16ZsGreen ($n = 7$ per group; $^*P < 0.05$, unpaired t-test). **k**, Frequency of ZsGreen$^+$ macrophages in lungs of wild-type and CCR2-knockout mice 24 h after injection with B16ZsGreen ($n = 4$ per group; $^*P < 0.05$ by unpaired t-test). **l**, Frequency of ZsGreen$^+$ CD103$^+$ cDCs in lungs of wild-type and CCR2-knockout mice 24 h after injection with B16ZsGreen ($n = 4$ per group; $^*P < 0.05$, unpaired t-test). **m**, **n**, Frequency (**m**) and absolute number (**n**) of CD8$^+$ T cells in lungs of wild-type or CCR20-knockout mice from **k** ($n = 4$ per group; $^*P < 0.05$, unpaired t-test). **o**, Representative images of lungs from Zbtb46-DTR bone marrow chimaeras treated with phosphate buffered saline (PBS) or diphtheria toxin (DT). Lungs collected 2 weeks after injection with B16ZsGreen. **p**, Total number of lung metastases in PBS- or DT-treated Zbtb46-DTR bone marrow chimaeras 2 weeks after injection with B16ZsGreen ($n = 5$ for PBS and 10 for DT groups, respectively; $^*P < 0.05$, unpaired t-test). Horizontal bars represent means, error bars are s.d.

in the mediastinal lymph node (mLN) revealed that all ZsGreen$^+$ cells were contained within the migratory CD103$^+$ DC population[17] (Fig. 4f–g). We thus imaged live mLN explants from CD11c-mCherry reporter mice (labelling DC and macrophages through expression of mCherry under control of the *Cd11c* promoter), 72 h after injection with B16F10 cells expressing ZsGreen and the ovalbumin peptide SL8 (B16ZsGreenSL8.) We found clusters of mCherry$^+$ APCs with ZsGreen puncta, clustered with transferred ovalbumin-specific CD8$^+$ (OT-I) T cells. The T cells exhibited a blast-like morphology, suggesting *in vivo* activation of T cells by DCs within the mLN (Fig. 4h and Supplementary Video 10). These data support a model whereby CD103$^+$ DCs acquire tumour material in the lung and subsequently migrate to the mLN to engage with cognate T cells. *In vitro*, CD103$^+$ DCs (isolated from mLN of metastasis-bearing mice at 72 h) were superior in their ability to activate OT-I T cells (Extended Data Fig. 6a–d). In contrast, neither CD11b$^+$ DCs nor CD8$^+$ DCs were observed to contain ZsGreen and were unable to stimulate OT-I T cells *in vitro* (Extended Data Fig. 6a–d).

Previous studies have highlighted the importance of the CCR2–CCL2 axis in monocyte recruitment to seed pro-tumour macrophage populations in the lung[4]. Analysis of CCR2-knockout animals, which recruit significantly fewer monocytes, and consequently macrophages[4], at two weeks after injection with B16ZsGreen, confirmed that CCR2-knockout hosts developed significantly fewer metastases (Fig. 4i, j). By characterizing ZsGreen$^+$ cells at 24 h, we observed a shift in cytoplast loading towards the immunostimulatory CD103$^+$ DCs (Fig. 4k, l). Moreover, in CCR2-knockout animals, we found a substantial increase both in the frequency and number of CD8$^+$ T cells in the lung (Fig. 4m, n). We thus considered whether host-protective CD103$^+$ DCs operate in competition with the pro-tumour macrophages.

To test the idea that metastatic success is specifically opposed by cDCs, we generated Zbtb46-DTR (expression of diphtheria toxin under control of the cDC-specific *Zbtb46* promoter)[18] bone marrow chimaeras. This permitted us to specifically and temporally deplete cDCs. We evaluated the metastatic burden in lungs two weeks after injection with B16ZsGreen; cDC-depleted animals developed sixfold more metastases than the non-depleted controls (Fig. 4o, p). We repeated these experiments in the presence of a subdermal primary tumour, mimicking the endogenous state of tumour metastasis with identical results (Extended Data Fig. 7). These data clearly establish that, despite relative rarity in the tumour interacting pool, lung-resident cDCs have a major role in restricting metastasis.

Previous research into how lung immune responses dictate metastatic success has been largely limited to recruited myeloid populations. This is evidenced by a recent review of the literature[2] that detailed 28 distinct primary articles focused on the function of recruited immune cells in the lung during metastasis and no references defining a role for resident immune cells. Although our analysis of tumour-interacting myeloid cells strongly supports waves of recruited neutrophils, monocytes and macrophages as populations of interest in the early metastatic niche, it also reveals the presence of rare lung-resident cDC subsets within the early interacting pool that mediate potent anti-metastatic effects. A recent study from our lab[19] identified a similarly rare CD103$^+$ cDC population acting locally in primary tumours to stimulate CD8$^+$ T cells providing adaptive protection. This suggests that novel immunotherapeutics designed to enhance these DC populations may provide a single strategy to modulate both primary and metastatic responses. This real-time study, like others of its kind, also highlights the value of direct observation as a means to identify how tumours interact with the colonized tissue, in this case by feeding material from the first pioneer cells into specific subsets of local and recruited myeloid populations.

Online Content Methods, along with any additional Extended Data display items and Source Data, are available in the online version of the paper; references unique to these sections appear only in the online paper.

Received 19 March 2015; accepted 12 January 2016.
Published online 16 March 2016.

1. Nguyen, D. X., Bos, P. D. & Massague, J. Metastasis: from dissemination to organ-specific colonization. *Nature Rev. Cancer* **9,** 274–284 (2009).
2. Kitamura, T., Qian, B. Z. & Pollard, J. W. Immune cell promotion of metastasis. *Nature Rev. Immunol.* **15,** 73–86 (2015).
3. Qian, B. *et al.* A distinct macrophage population mediates metastatic breast cancer cell extravasation, establishment and growth. *PLoS ONE* **4,** e6562 (2009).
4. Qian, B. Z. *et al.* CCL2 recruits inflammatory monocytes to facilitate breast-tumour metastasis. *Nature* **475,** 222–225 (2011).
5. Kaplan, R. N. *et al.* VEGFR1-positive haematopoietic bone marrow progenitors initiate the pre-metastatic niche. *Nature* **438,** 820–827 (2005).
6. Looney, M. R. *et al.* Stabilized imaging of immune surveillance in the mouse lung. *Nature Methods* **8,** 91–96 (2011).
7. Peinado, H. *et al.* Melanoma exosomes educate bone marrow progenitor cells toward a pro-metastatic phenotype through MET. *Nature Med.* **18,** 883–891 (2012).
8. Joyce, J. A. & Pollard, J. W. Microenvironmental regulation of metastasis. *Nature Rev. Cancer* **9,** 239–252 (2009).
9. Raposo, G. & Stoorvogel, W. Extracellular vesicles: exosomes, microvesicles, and friends. *J. Cell Biol.* **200,** 373–383 (2013).
10. Di Vizio, D. *et al.* Oncosome formation in prostate cancer: association with a region of frequent chromosomal deletion in metastatic disease. *Cancer Res.* **69,** 5601–5609 (2009).
11. Mendoza, A. *et al.* Modeling metastasis biology and therapy in real time in the mouse lung. *J. Clin. Invest.* **120,** 2979–2988 (2010).
12. Al-Mehdi, A. B. *et al.* Intravascular origin of metastasis from the proliferation of endothelium-attached tumor cells: a new model for metastasis. *Nature Med.* **6,** 100–102 (2000).
13. Thornton, E. E. *et al.* Spatiotemporally separated antigen uptake by alveolar dendritic cells and airway presentation to T cells in the lung. *J. Exp. Med.* **209,** 1183–1199 (2012).
14. Ovchinnikov, D. A. *et al.* Expression of Gal4-dependent transgenes in cells of the mononuclear phagocyte system labeled with enhanced cyan fluorescent protein using *Csf1r*-Gal4VP16/UAS-ECFP double-transgenic mice. *J. Leukoc. Biol.* **83,** 430–433 (2008).
15. Anderson, K. G. *et al.* Intravascular staining for discrimination of vascular and tissue leukocytes. *Nature Protocols* **9,** 209–222 (2014).
16. Jakubzick, C. *et al.* Minimal differentiation of classical monocytes as they survey steady-state tissues and transport antigen to lymph nodes. *Immunity* **39,** 599–610 (2013).
17. Idoyaga, J. *et al.* Specialized role of migratory dendritic cells in peripheral tolerance induction. *J. Clin. Invest.* **123,** 844–854 (2013).
18. Meredith, M. M. *et al.* Expression of the zinc finger transcription factor zDC (Zbtb46, Btbd4) defines the classical dendritic cell lineage. *J. Exp. Med.* **209,** 1153–1165 (2012).
19. Broz, M. L. *et al.* Dissecting the tumor myeloid compartment reveals rare activating antigen-presenting cells critical for T cell immunity. *Cancer Cell* **26,** 638–652 (2014).

Supplementary Information is available in the online version of the paper.

Acknowledgements We thank D. Hume for providing MacBlue mice; Z. Werb for providing MDA-MB231 GFP cells; J. Massegue and S. Abrams for providing PyMT-B cells; J. Cyster for providing us with CCR2-knockout mice. We would also like to thank E. Thornton for her initial work in developing lung intravital imaging. M. Werner for early technical assistance in this project. All members of the Krummel laboratory, BIDC, and M Koch for discussion, support, and guidance while developing this work. This work was supported in part by a Department of Defense post-doctoral fellowship to M.B.H. (W81XWH-13-1-0009) and NIH grants U54 CA163123, P01 HL024136 and R21CA167601.

Author Contributions M.B.H. designed and conducted most of the experiments, data analysis, and drafted the manuscript; A.B. developed the Intercostal Imaging Window; A.N. generated B16ZsGreen cell line and discussed data; E.W.R. generated mTmG mouse embryonic fibroblasts and provided editorial support on manuscript; M.L.R. participated in development and troubleshooting of LIVM method, discussed data and project direction; A.G. participated in intravital LN experiments and provided editorial support on manuscript. M.F.K. designed experiments, interpreted data, and with other authors, developed the completed manuscript.

Author Information Reprints and permissions information is available at www.nature.com/reprints. The authors declare no competing financial interests. Readers are welcome to comment on the online version of the paper. Correspondence and requests for materials should be addressed to M.F.K. (matthew.krummel@ucsf.edu).

METHODS

Mice. Mice were housed and bred under specific pathogen-free conditions at the University of California, San Francisco Laboratory Animal Research Center and all experiments conformed to ethical principles and guidelines approved by the UCSF Institutional Animal Care and Use Committee. C57/BL6 mice were purchased from Simonsen Laboratories or bred in house, and unless otherwise noted animals used were male between 6–8 weeks of age. Actin–CFP[20] mice were obtained from I. Weissman (Stanford University). MacBlue[14] mice were a gift from D. Hume (The Roslin Institute). CD11c-mCherry[21] mice were a gift from L. Lefrancois (University of Connecticut). CCR2-knockout[22] mice were a gift from J. Cyster. mTmG[23], Nur77-GFP[24], and Zbtb46-DTR[18] mice were purchased from Jackson Laboratories.

Cell lines. B16F10 (ATCC), PyMT-B[25,26] was a gift from J. Massegue and S. Abrams, MDA-MB231-expressing GFP was a gift from Z. Werb, mouse embryonic fibroblasts were prepared from mTmG mice as follows. Day 13.5 embryos were collected from pregnant mTmG females. Following removal of fetal liver embryos, were minced and subjected to Trypsin digestion. The retrieved cells were washed and resuspended in DMEM (GIBCO) and 10% heat-inactivated FCS and L-glutamate with penicillin and streptomycin. Cells were plated and passaged overnight. Media was aspirated after 24 h to remove any cells remaining in suspension and replaced with fresh media. Cells were then grown to 70%–80% confluency and cryopreserved. For experimental use, a vial of mouse embryonic fibroblasts were thawed and grown to 80% confluency in fresh media and used immediately for experiments. ZsGreen- and DsRed-expressing cells lines were generated by retroviral transduction with empty pSiren–ZsGreen (Clontech) or pSiren–DsRED(Clontech). Retrovirus was generated in Phoenix packaging cells (as previously described[27]) and applied to sub-confluent B16F10 or PyMT-B cells. Transduced cells were sorted for fluorescent-protein-positive cells on day 2 after infection on a FACSAria III sorter. Following an additional week of culture, cells were sorted a second time to ensure faithful expression of the reporter. Cell lines were subsequently tested and confirmed to be mycoplasma free by PCR.

Metastasis induction. For intravital imaging, flow cytometry and T cell activation assay sorting experiments, cultured B16ZsGreen cells were collected with Trypsin/EDTA and cultured for 30 min at 37 °C in complete media with or without Hoechst-3342 (Molecular Probes) at 1 $\mu g\,ml^{-1}$ to stain for nuclei and/or recover cells after collection. Cells were subsequently washed $\times 2$ in PBS and 5×10^5 cells were injected via the tail vein into mice. For metastasis quantification experiments between 1×10^5 and 2.5×10^5 B16ZsGreen cells, prepared in the same fashion, were injected via the tail vein.

Intravital imaging of pulmonary metastasis via intercostal insertion window. This is a modified version of our previously published method of stabilized lung imaging[6], modifications are as follows. Mice were anaesthetized with 2.5% Avertin at a dose of 10 $\mu l\,g^{-1}$ and secured with tape to a custom heated microscope stage. Tracheostomy was performed to insert a small tracheal cannula, which was sutured into place and attached to a MiniVent mouse ventilator (Harvard Apparatus). Mice were ventilated with a stroke volume of 10 μl of compressed air (20–22% O_2) per gram of mouse weight, a respiratory rate of 130–140 breaths per minute, and a positive-end expiratory pressure of 2.5–3 cm H_2O. Isoflurane was continuously delivered at 1.5% to maintain anaesthesia and mice were given i.v. Lactated Ringers Solution (Baxter Health Care) at a rate of 0.8–1.6 $\mu l\,min^{-1}$ continuously during imaging. The mice were then placed in the right lateral decubitus position and a small surgical incision was made to expose the rib cage. A second incision was then made into the intercostal space between ribs 4 and 5, through the parietal pleura, to expose the surface of the left lung lobe. A flanged thoracic suction window with 8 mm coverslip (Extended Data Fig. 2) was then inserted between the two ribs and secured to the stage using a set of two optical posts and a 90° angle post clamp (Thor Labs). 20–25 mm Hg of suction was applied (Amvex Corporation) to gently immobilize the lung. The two-photon microscope objective was then lowered into place over the thoracic suction window. For imaging of the arrival of metastatic tumour cells, 5×10^5 B16F10 cells expressing ZsGreen were injected inline through the i.v. line during imaging. In experiments where metastatic cells were imaged at later time points (6–24 h), cells were instead injected i.v. through a tail vein injection at the appropriate time point before performing the intravital imaging surgery.

Two-photon microscopy. Intravital imaging was performed using a custom-built two-photon setup equipped with two infrared lasers (MaiTai, Spectra Physics; Chameleon, Coherent). The MaiTai laser was tuned to 810 nm for excitation of CFP. Chameleon laser excitation was tuned to 980 nm for simultaneous excitation of TdTomato or mCherry and ZsGreen and/or GFP. Emitted light was detected using a 25× 1.2NA water lens (Zeiss) coupled to a 6-colour detector array (custom; using Hamamatsu H9433MOD detectors). Emission filters used were: blue 475/23, green 510/42, yellow 542/27, red 607/70, far red 675/67. The microscope was controlled by the MicroManager software suite, *z*-stack images were acquired with fourfold averaging and *z*-depths of 3 μm Data analysis was performed using the Imaris software suite (Bitplane).

Non-shear lung slice imaging. Slice imaging was performed as previously described[13]. In brief, mice were injected with 5×10^5 B16ZsGreen cells by tail vein. After 1 h mice were euthanized by anaesthetic overdose (1 ml of 2.5% Avertin), mice were then intubated by tracheotomy with the sheath from an 18-gauge i.v. catheter. Lungs were subsequently inflated with 1 ml of 2% low melting temp agarose (BMA) in sterile PBS at 37 °C. Agarose was then solidified by flooding the chest cavity with 4 °C PBS. Inflated lungs were excised and the left lobe was cut into ~300-μm sections using a vibratome. Sections were mounted on plastic coverslips and imaged by two-photon microscopy at 37 °C in carbogen (5% CO_2:95% O_2)-perfused RPMI-1640 media (Gibco, without Phenol Red).

Lymphnode explant imaging. Explant imaging was performed as previously described[28]. In brief, 2 million GFP-expressing OT-I T cells were transferred in CD11c-mCherry mice 1 day before injection with 5×10^5 B16ZsGreenSL8 cells via tail vein. Mediastinal lymph node was removed, cleaned of fat, and immobilized on a plastic coverslip with the hilum facing away from the objective. Lymph nodes were imaged in 30-min intervals with 810 nm excitation on a two-photon microscope, as above.

Tissue digests for flow cytometry and sorting. Lungs were collected from mice following euthanasia by overdose with 2.5% Avertin. Lungs were placed in 5 ml of DMEM (GIBCO) with 0.26 U ml^{-1} LiberaseTM (Roche) and 0.25 mg ml^{-1} DNaseI (Roche). Samples were placed in C-Tubes (Miltenyi) and briefly processed with a GentleMACS Dissociator (Miltenyi). Samples were then incubated at 37 °C for 30 min and processed a second time via GentleMACS. Tissue homogenate was then passed through a 100 μm Nytex Filter. Red blood cells were lysed with 3 ml of 175 mM NH_4Cl per lung for 5 min at 37 °C. Samples were then filtered through a 40 μm Nytex filter and resuspended for subsequent FACS staining. For experiments where vascular localization was assessed, mice were injected with i.v. 10 μg CD45–APC (allophycocyanin; eBioscience Clone 30-F11) 5 min before collection and prepared as per the previously published protocol[15]. Lymph nodes were prepared by placing in 1 ml of digestion buffer and puncturing with sharp forceps. Samples were incubated for 15 min at 37 °C and then pipetted up and down ~20 times with a P1000 pipette to dissociate. Samples were returned to 37 °C for 15 min. Cell suspension was then filtered through a 40 μm Nytex filter and prepared for subsequent FACS staining.

Flow cytometry. For surface staining, cells were incubated with anti-Fc receptor antibody (clone 2.4G2) and stained with antibodies in PBS and 2% fetal calf serum for 30 min on ice. Viability was assessed by staining with fixable Live/Dead Zombie NIR (Biolegend) or 4′,6-diamidino-2-phenylindole (Molecular Probes). All flow cytometry was performed on a BD Fortessa flow cytometer. Analysis of flow cytometry data was performed using Flowjo (Treestar). Cell sorting was performed using a BD FACS Aria II or a BD FACS Aria III.

Antibody clones used in these studies: CD45-Alexa 700 (eBioscience clone 30-F11), MHCII Brilliant Violet 421 (Biolegend clone M5/114.15.2), CD11c Brilliant Violet 510 (Biolegend clone N418), CD11b Brilliant Violet 605 or PerCPCy5.5 (Biolegend clone M1/70), Ly6C Brilliant Violet 711 (Biolegend clone HK1.4), CD24 PeCy7 (Biolegend clone M1/69), CD103 PE (Biolegend clone 2E7), CD69 PeCy7 (H1.2F3) Ly6G A647 (Biolegend 1A8), Siglec-F A647 (BD Bioscience clone E50-2440), CD19 A647 (Biolegend clone 6D5), CD90.2 A647 (Biolegend clone 30.H12), VCAM-1 PE (Biolegend clone 429), CD88 PE (Biolegend clone 20/70), CD155 PE (Biolegend clone 4.24.1), CMKLR1 PE (Biolegend clone BZ194), CD38 PE (Biolegend clone 14.27), CD63 PE (Biolegend clone NVG-2) was performed in FACS buffer for 20 min at 4 °C. Live/Dead discrimination was performed using either Propidium Iodide or Zombie NIR Fixable Live/Dead Stain (Biolegend). Samples were analysed on a LSRFortessa (BD Biosciences) in the UCSF Flow Cytometry Core.

T-cell activation assay. Assays were performed as previously published[19]. In brief, lymph node cells from OT-I TCR transgenic mice were isolated and were enriched for naive $CD8^+$ T cells by StemSep CD8 enrichment (Stemcell Technologies). Naive OT-I CD8 cells or labelled with 2 μM succinimidyl ester eFluor 670 (SE670, eBioscience) and mixed with APC at a 10:1 ratio (1,0000 T cells: 1,000 APC) with unpulsed mLN antigen-presenting cells (sorted from the lymph node 72 h following injection with either B16ZsGreenSL8 or B78mCherryOVA) in 96-well V-bottom plates for either 24 or 72 h at 37 °C in 5% CO_2, at which point activation was measured by CD69 and Nur77-GFP upregulation and SE670 dilution using flow cytometry.

Zbtb46-DTR bone marrow chimaeras. In order to avoid mortality associated with diphtheria-toxin-mediated depletion of Zbtb46-DTR expressing cells in intact animals[18], we generated bone marrow chimaeras. Bone marrow cells (3×10^6) from Zbtb46-DTR mice were adoptively transferred retro-orbitally into lethally irradiated recipients. Animals were allowed to recover and repopulate the haematopoietic compartment for 8 weeks. On day 1, animals were injected with

20 ng of diphtheria toxin in PBS or an equivalent volume of PBS alone. On day 0, animals were injected with 150,000 B16ZsGreen cells via tail vein injection. On day +1, animals were injected with a second dose of 20 ng of diphtheria toxin or PBS. Metastases were then allowed to develop for 2 weeks before quantification, as described elsewhere in these methods. In alternate experiments, mice were first injected with 1×10^5 B16F10 cells in growth factor reduced Matrigel (Corning, 50 μl of 50% Matrigel diluted in PBS) 3 weeks before diphtheria toxin and metastasis injection injection as per the above protocol. Primary tumours were not allowed to exceed 2 cm before euthanasia in accordance with University of California, San Francisco Institutional Animal Care and Use Committee protocol, as such in these experiments metastases were collected at 1 week to fit within bounds of primary tumour endpoint criteria.

Assessment of cell activity. Data for tumour cells of interest collected from intravital imaging of lung was used for these analyses. Tumour cells were assessed for a 30 min interval at either 2 h or 24 h after injection. Data were first subjected to a maximum intensity projection and output data was binarized at each time point to reveal the maximum boundaries of the cell at any given time point. Data was then projected over time to yield an image depicting the total area occupied by the cell over the 30 min window. Areas were then calculated for the total area of the time projection, as well as the common area colocalized between the initial time point (T0), the final time point (T30) and the time projection (T-Project) to yield the parameter T-Overlap. The cell activity index was then calculated as Cell Activity Index = T-Project/T-Overlap.

Image and statistical analysis. All image analysis was performed using Imaris (Bitplane) in conjuction with Matlab (Mathworks). For statistical analysis, unless otherwise noted, all data were expressed as mean ± s.d. Comparisons between groups were analysed with by *t*-test, multi-group comparisons were performed using a one-way ANOVA test and Bonferroni post-hoc test, using Graphpad Prism software. In all cases where statistical significance is provided, variance was not statistically different between groups with the exception of Fig. 1h. Sample sizes were chosen on the basis of previous experience in the lab with respect to inherent variability in i.v. metastatic models and intravital imaging. Animals within each cohort were randomly assigned to treatment groups. In cases where wild-type mice (Simonsen) were used, entire cages were randomly assigned into treatment groups. Blinded analysis was not performed in these studies. Data were considered as statistically significant when P values were <0.05, indicated by '*' in figures, unless otherwise noted. $t_{1/2}$ value was calculated as the half-life (ln(2)/(K); where K is the rate constant of the regression) of a one-phase exponential decay nonlinear regression.

20. Hadjantonakis, A. K., Macmaster, S. & Nagy, A. Embryonic stem cells and mice expressing different GFP variants for multiple non-invasive reporter usage within a single animal. *BMC Biotechnol.* **2,** 11 (2002).
21. Khanna, K. M. *et al.* T cell and APC dynamics in situ control the outcome of vaccination. *J. Immunol.* **185,** 239–252 (2010).
22. Boring, L. *et al.* Impaired monocyte migration and reduced type 1 (Th1) cytokine responses in C–C chemokine receptor 2 knockout mice. *J. Clin. Invest.* **100,** 2552–2561 (1997).
23. Muzumdar, M. D., Tasic, B., Miyamichi, K., Li, L. & Luo, L. A global double-fluorescent Cre reporter mouse. *Genesis* **45,** 593–605 (2007).
24. Moran, A. E. *et al.* T cell receptor signal strength in T_{reg} and iNKT cell development demonstrated by a novel fluorescent reporter mouse. *J. Exp. Med.* **208,** 1279–1289 (2011).
25. Stewart, T. J. & Abrams, S. I. Altered immune function during long-term host-tumor interactions can be modulated to retard autochthonous neoplastic growth. *J. Immunol.* **179,** 2851–2859 (2007).
26. Acharyya, S. *et al.* A CXCL1 paracrine network links cancer chemoresistance and metastasis. *Cell* **150,** 165–178 (2012).
27. Friedman, R. S., Jacobelli, J. & Krummel, M. F. Surface-bound chemokines capture and prime T cells for synapse formation. *Nature Immunol.* **7,** 1101–1108 (2006).
28. Gérard, A. *et al.* Secondary T cell–T cell synaptic interactions drive the differentiation of protective $CD8^+$ T cells. *Nature Immunol.* **14,** 356–363 (2013).

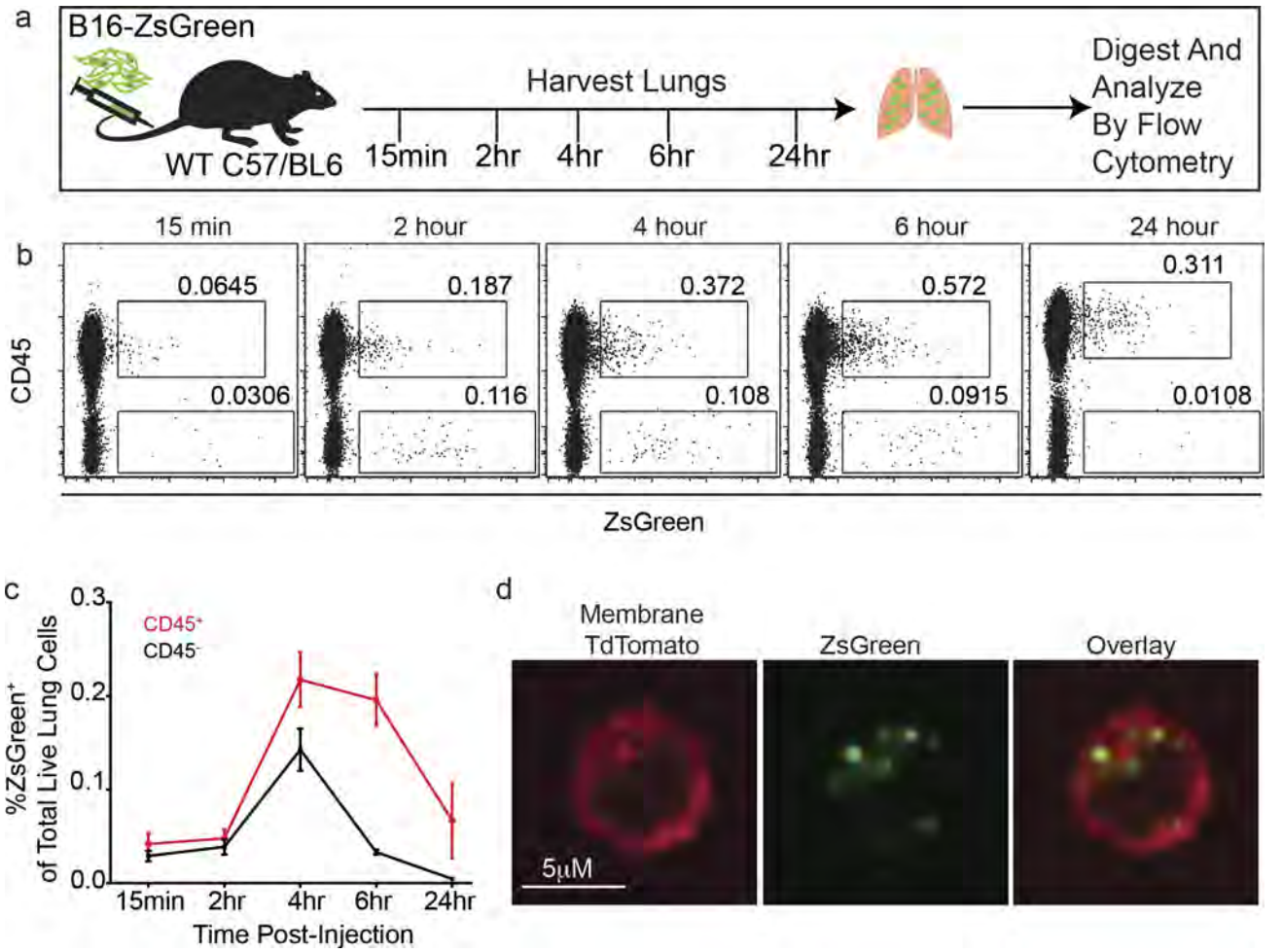

Extended Data Figure 1 | Loading of lung immune cells by prospective metastatic B16 melanoma. a, Schema for assessing immune cell loading by i.v.-injected B16ZsGreen cells. **b**, Representative plots of ZsGreen$^+$ populations in the lungs of mice injected with B16ZsGreen over the first 24 h following injection. Data are gated on the basis of expression of the immune cell marker CD45. **c**, Quantification of **b** with $n = 6$ per group, error bars are s.d. **d**, Confocal imaging of CD45$^+$ZsGreen$^+$ cells sorted from a lung digest from a ubiquitous membrane-bound TdTomato fluorescent mouse 24 h after i.v. injection with B16ZsGreen.

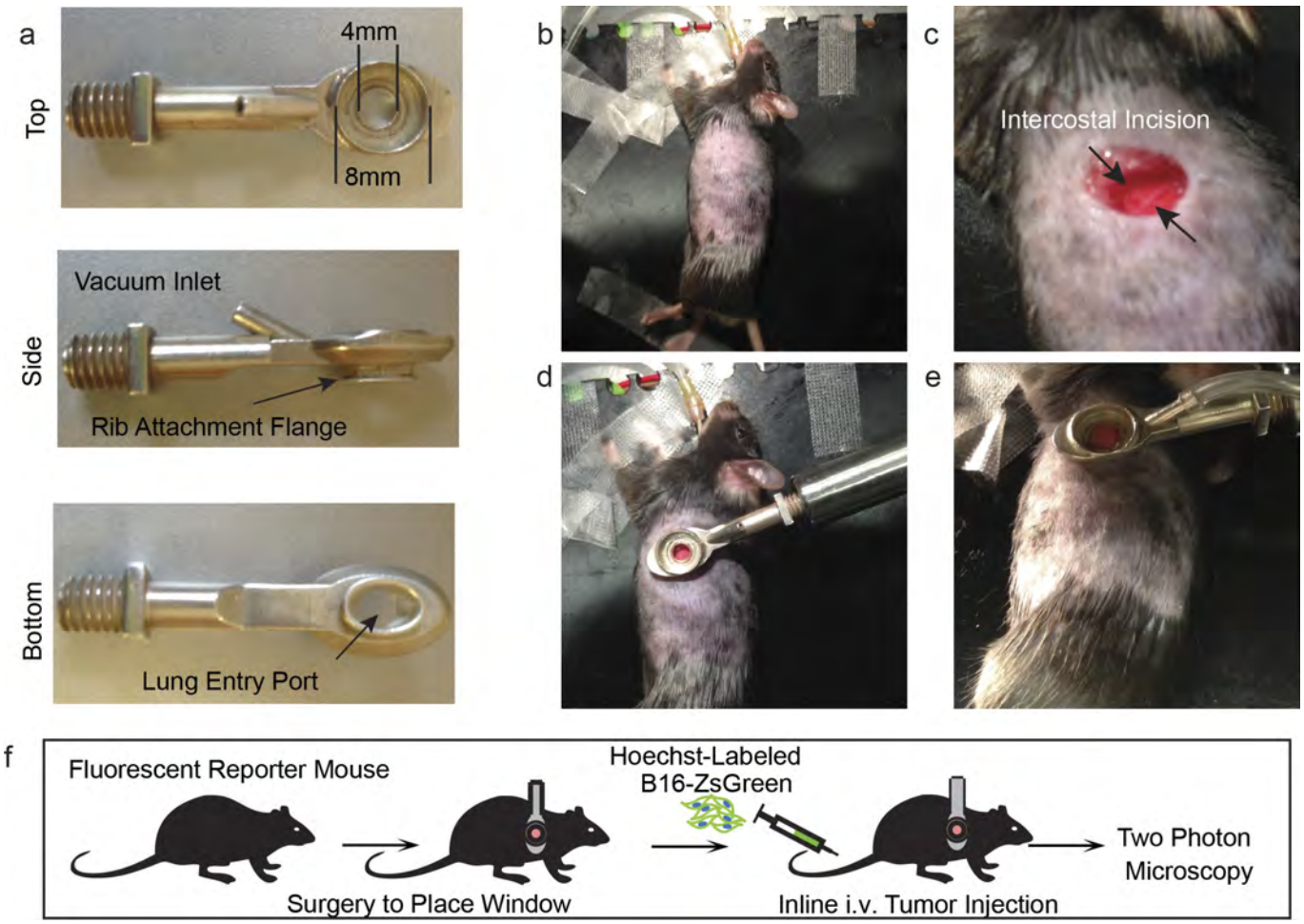

Extended Data Figure 2 | Intercostal insertion window for lung intravital microscopy. a, Top, side, and bottom views of the intercostal insertion window. The window accommodates an 8 mm coverslip and allows for visualization of a 4 mm field of the left lung lobe. **b**–**e**, Images detailing surgical insertion of the intercostal window. **b**, Mouse is intubated, attached to ventilator, and placed in right lateral decubitis position and surgical field is shaved. **c**, An ~6 mm incision is made immediately above ribs 4 and 5 over the anterior surface of left lung lobe. **d**, The intercostal window is slipped between ribs 4 and 5, and attached to a rigid support. **e**, Around 20 mm Hg of vacuum suction is applied to the window to secure a small portion of lung to the coverglass. **f**, Schema showing approach for two-photon intravital microscopy of lung seeding by B16ZsGreen cells.

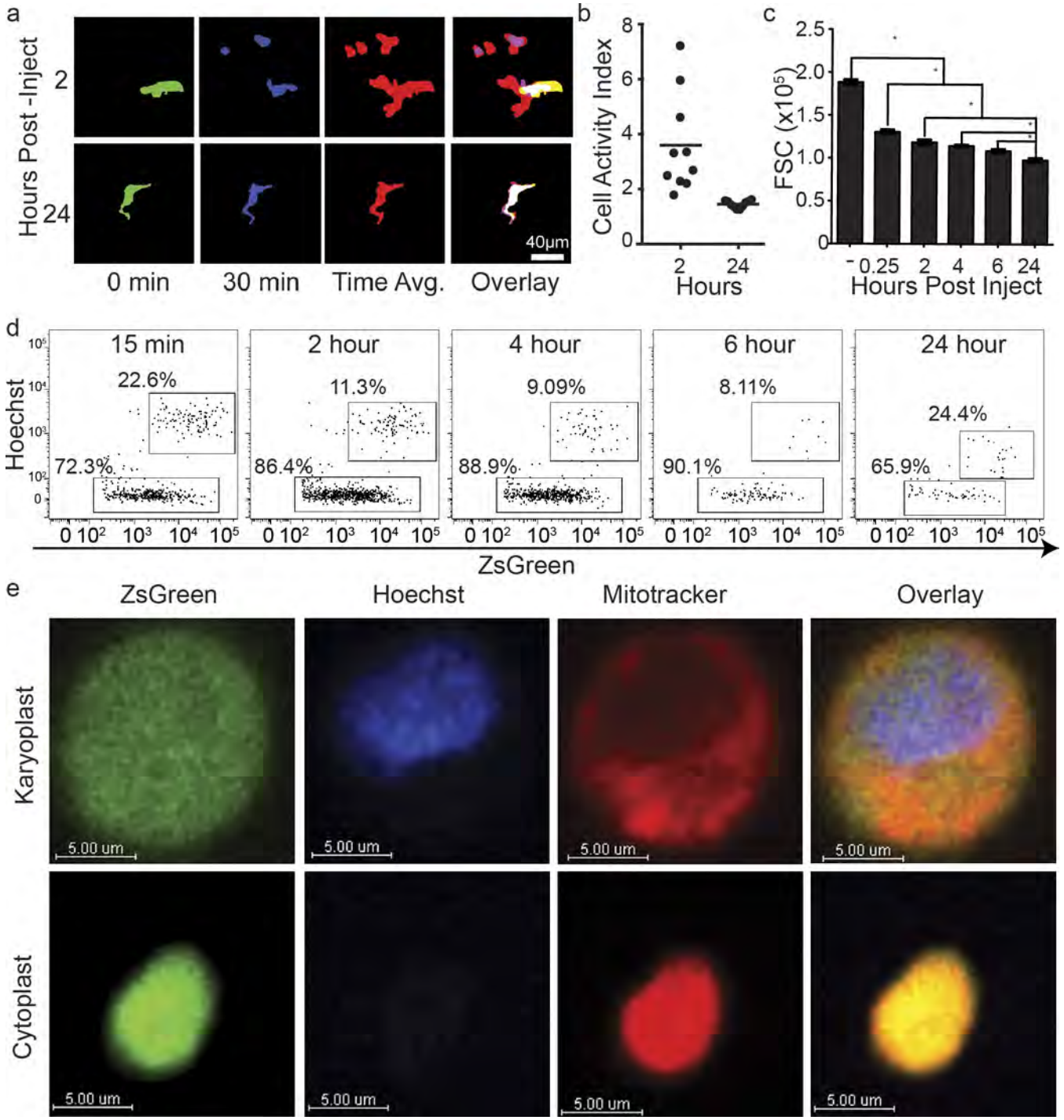

Extended Data Figure 3 | Assessment of tumour cell activity and cytoplast characterization. a, Binarized maximum intensity projections of representative cells at 2 or 24 h after injection. Cells were time-projected over a 30 min window to assess overall cellular activity during the interval. Images show the beginning time point (0 min), the ending time point (30 min), the time projection, and the overlay. White-filled space in the overlay represents the region of the cell that was stable during the analysed interval. These data are associated with Supplementary Video 3. These data are representative from imaging performed in 3 mice. **b**, Quantification of the cell activity index (defined as the area calculated from the projection of all positions over time as a ratio of the common area over all time (for example, area of overlap)) from analysis in **d** ($n = 10$ cells per group, horizontal bars are mean value). **c**, Flow cytometric quantification of FSC for tumour cells isolated from lung via digestion at 15 min, 2 h, 4 h, 6 h, and 24 h after injection. $^*P < 0.05$, one-way ANOVA with Bonferroni post-hoc test, error bars are s.d. **d**, Representative data from flow cytometric discrimination of nucleated karyoplasts and anucleate cytoplasts derived from B16ZsGreen tumour cells in the lung *in vivo* over a 24 h time course, full data set quantified in Fig. 1e. **e**, confocal analysis of Hoechst and Mitotracker-labelled B16ZsGreen karyoplasts and cytoplasts sorted from *in vitro* culture of B16ZsGreen cells.

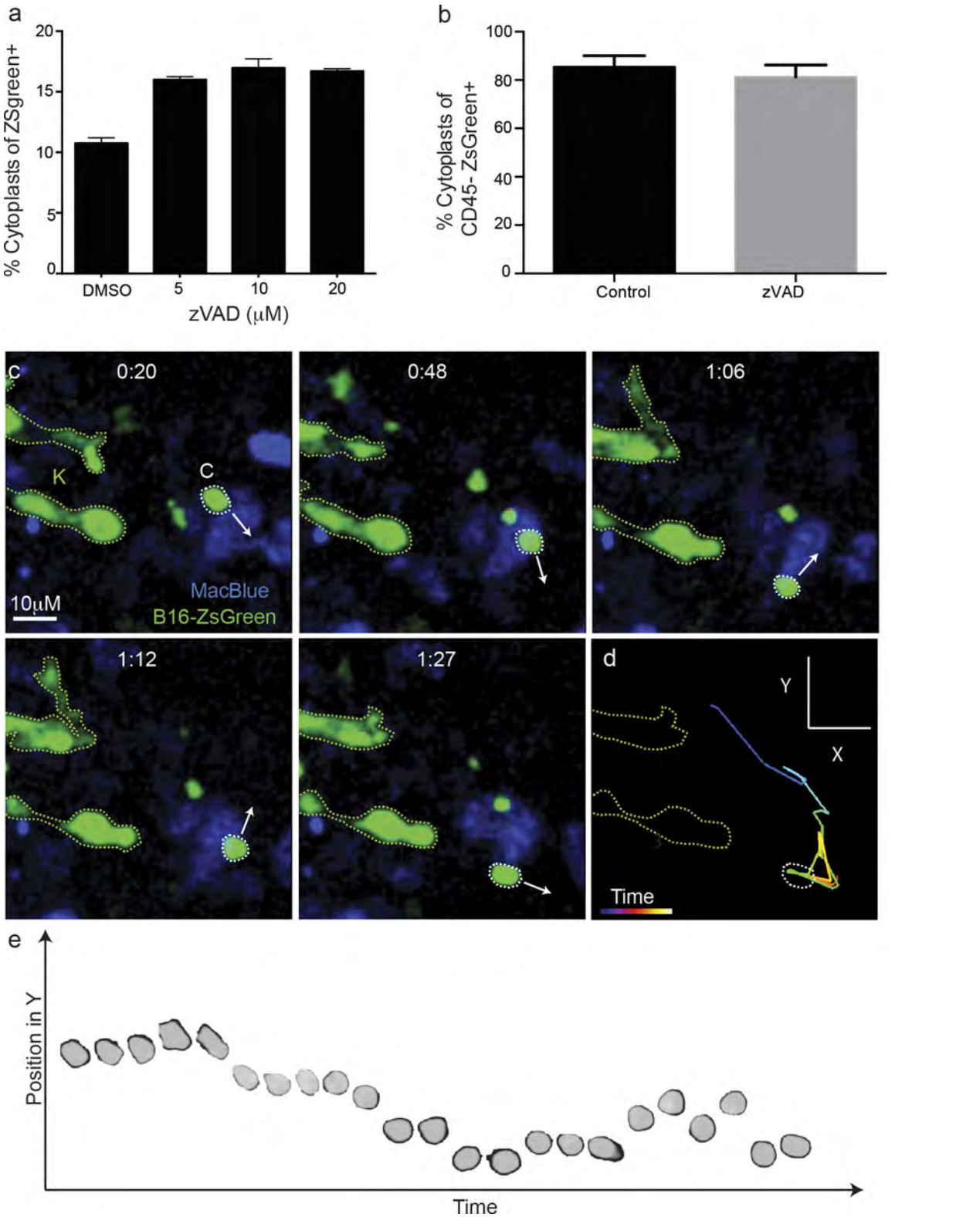

Extended Data Figure 4 | Autonomous motility of cytoplasts *in vivo*. **a**, Flow cytometric quantification of cytoplasts *in vitro* following 24 h treatment with Z-VAD at indicated concentrations. **b**, Flow cytometric quantification of cytoplasts *in vivo* from lung digests of mice treated with 10 μg Z-VAD i.v at the time of injection with 2.5×10^5 B15ZsGreen cells (**a** and **b**, $n = 4$ per group; no significant difference detected between groups, unpaired *t*-test, error bars are s.d.). **c**, Image series for B16ZsGreen cytoplast migrating autonomously through the lung microvasculature of a MacBlue host. Arrows represent the direction of the trajectory of the cytoplast at indicated time point. These data are associated with Supplementary Video 6. These data are representative of imaging collected from at least 12 mice. **d**, Representative tracking of a cytoplast from Supplementary Video 6 (and Extended Data Fig. 4c). **e**, A superposition image of 23 consecutive time points of a cytoplast migrating through lung microvasculature. Image shows the change in position in the *y* axis of direction as defined in **d** at each subsequent timepoint as the cytoplast migrates up and down the vessel.

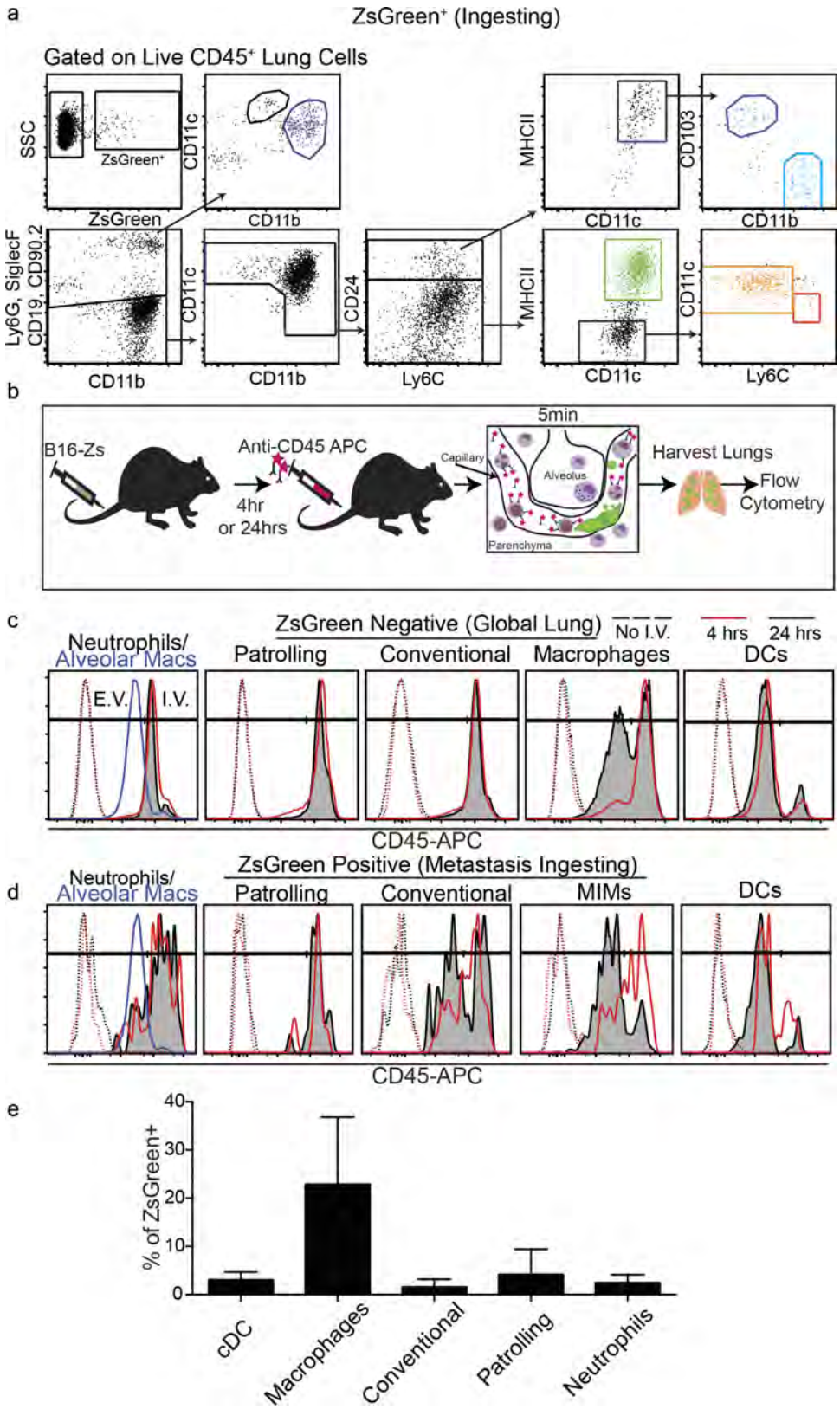

Extended Data Figure 5 | Characterization of tumour-interacting myeloid cell waves. a, Representative gating for total lung myeloid populations. **b**, Schema detailing method for discrimination of intravascular versus extravascular localization of lung myeloid populations. **c**, **d**, Representative histograms of intravascular CD45 staining used to discriminate between intravascular and extravascular localization of lung myeloid cells at 4 and 24 h after injection with B16ZsGreen. Data quantified in Fig. 3d. In the leftmost panels, alveolar macrophages at 24 h after tumour injection are shown as a known control for extravascular staining. **c**, Total lung myeloids. **d**, ZsGreen^{+} myeloid cells. **e**, Quantification ZsGreen^{+} myeloid populations by flow cytometry in lungs of mice bearing 2-week subdermal B16ZsGreen tumours ($n = 4$ per group). Error bars are s.d.

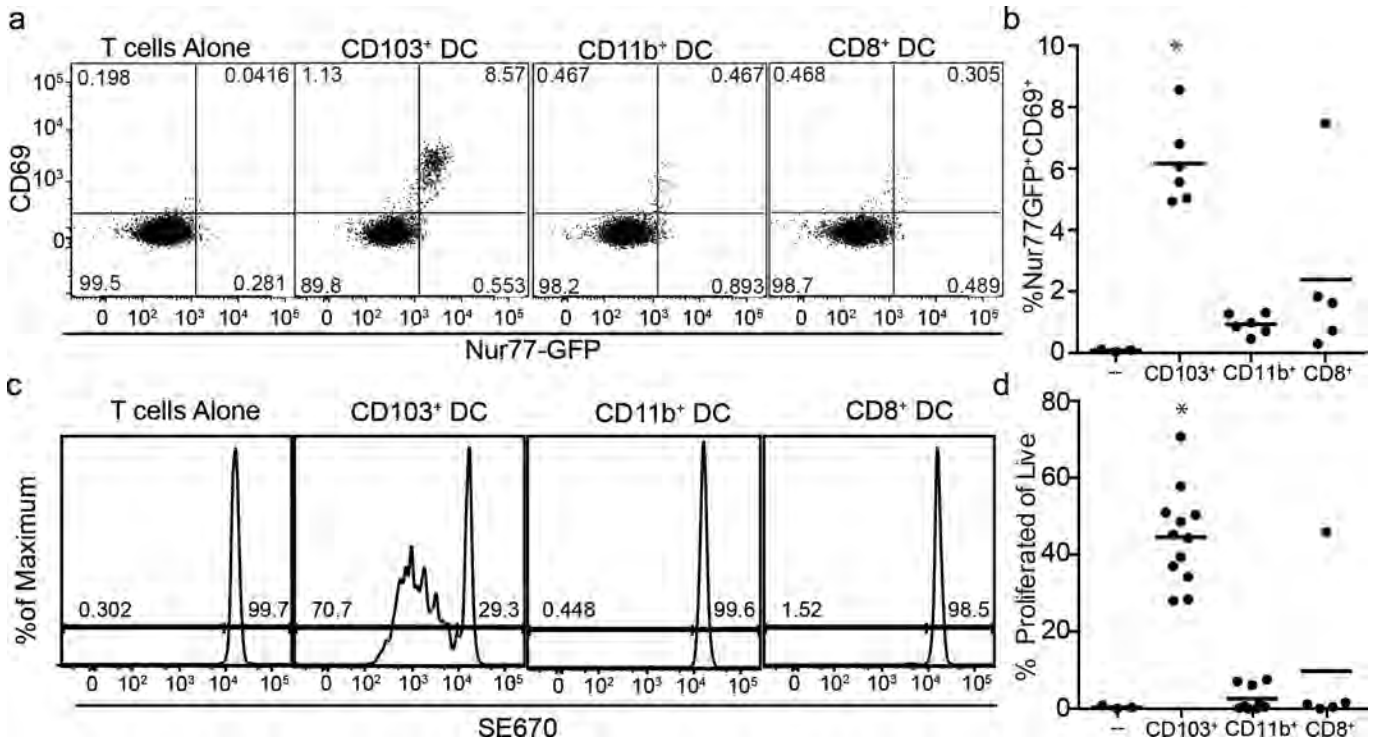

Extended Data Figure 6 | Stimulatory capacity of CD103$^+$ DCs in lung-draining lymph node. a, CD69 vs Nur77-GFP expression 24 h after culture from *ex vivo* coculture of OT-I TCR transgenic CD8$^+$ T cells with sorted APCs from mLNs, where the latter were isolated 72 h post-injection with B16ZsGreenSL8. **b**, Quantification of **a**. **c**, Dilution of SE670 as an index of proliferation 72 h after culture with indicated APC populations. **d**, Quantification of **c**. $n = 6$ (**b**) or 6–12 (**d**) per group from 2 experiments; $^*P < 0.05$, one-way ANOVA with Bonferroni post-hoc test, horizontal bars are mean value.

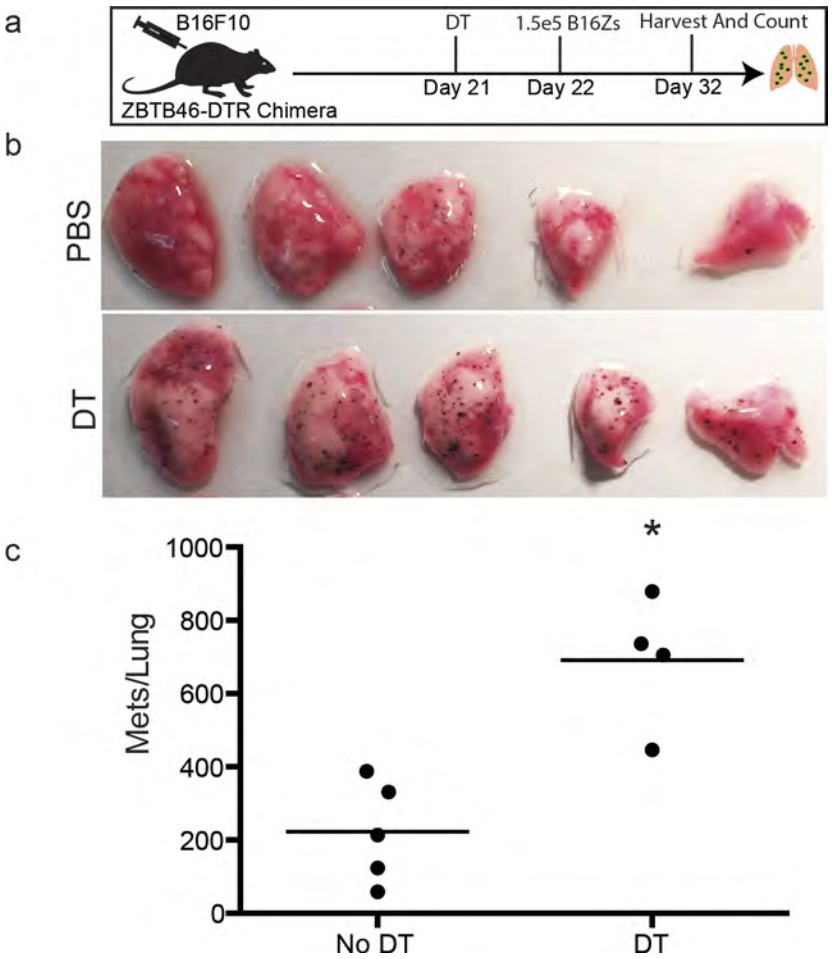

Extended Data Figure 7 | cDCs confer anti-metastatic activity in the presence of a primary tumour. a, Experimental schema for evaluation of role of cDCs in lung metastasis in the presence of a primary tumour. **b**, Representative images of lungs from Zbtb46-DTR bone marrow chimaeras treated with PBS or DT after implantation of a primary subdermal tumour (1×10^5 B16F10 in matrigel) and i.v. metastases (1.5×10^5 B16ZsGreen). Metastases were assessed one week after i.v. injection. **c**, Quantification of total number of visible ZsGreen$^+$ lung metastases in PBS- or DT-treated Zbtb46-DTR bone marrow chimaeras. $n = 4$–5 per group, representative of 2 experiments; $^*P < 0.05$, unpaired t-test, horizontal bars are mean value.